RESEARCH

Assessment of Laws of the Wall During Flame–Wall Interaction of Premixed Flames Within Turbulent Boundary Layers

Umair Ahmed[1] · Sanjeev Kr. Ghai[1] · Nilanjan Chakraborty[1]

Abstract

The validity of the usual laws of the wall for Favre mean values of the streamwise velocity component and temperature for non-reacting flows has been assessed for turbulent premixed flame-wall interaction using Direct Numerical Simulation (DNS) data. Two different DNS databases corresponding to friction velocity-based Reynolds number of 110 and 180 representing unsteady head-on quenching of statistically planar flames within turbulent boundary layers have been considered. The usual log-law based expressions for the Favre mean values of the streamwise velocity and temperature for the inertial layer have been found to be inadequate at capturing the corresponding variations obtained from DNS data. The underlying assumptions of constant shear stress and the equilibrium of production and dissipation of turbulent kinetic energy underpinning the derivation of the usual log-law for the mean streamwise velocity have been found to be rendered invalid within the usual inertial layer during flame-wall interaction for both cases considered here. The heat flux does not remain constant within the usual inertial layer, and the turbulent flux of temperature exhibits counter-gradient transport within the so-called inertial layer for the cases considered in this work. These render the assumptions behind the derivation of the usual log-law for temperature to be invalid for application to turbulent flame-wall interaction. It has been found that previously proposed empirical modifications to the existing laws of the wall, which account for density and kinematic viscosity variations with temperature, do not significantly improve the agreement with the corresponding DNS data in the inertial layer and the inaccurate approximations for the kinematic viscosity compensated wall normal distance and the density compensated streamwise velocity component contribute to this disagreement. The DNS data has been utilised here to propose new expressions for the kinematic viscosity compensated wall normal distance and the density compensated streamwise velocity component, which upon using in the empirically modified law of wall expressions have been demonstrated to provide reasonable agreement with DNS data.

Keywords Law of the wall · Log-law · Inertial layer · Turbulent boundary layer · Flame-wall interaction · Direct Numerical Simulations

✉ Nilanjan Chakraborty
nilanjan.chakraborty@ncl.ac.uk

1   School of Engineering, Newcastle University, Newcastle-Upon-Tyne NE1 7RU, UK

1 Introduction

Flame-wall interaction (FWI) is of fundamental importance for the analysis of heat transfer rates and thermal stresses experienced by combustor walls, and it is particularly important for the design process of modern downsized combustors and micro combustors where FWI takes place more readily than conventional combustors. Several studies have contributed to the fundamental understanding and modelling of FWI for premixed combustion using both experimental (Jainski et al. 2017a, b, 2018; Mann et al. 2014; Rißmann et al. 2016) and computational (Ahmed et al. 2018; Ahmed et al. 2019, 2020; Ahmed et al. 2021a, 2021b, 2021c, 2021d; Ahmed et al. 2023a, b; Ahmed et al. 2023b; Alshaalan and Rutland 2002; Alshaalan and Rutland 1998; Bruneaux et al. 1996; Bruneaux et al. 1997; Ghai et al. 2022b; Ghai et al. 2022c; Ghai et al. 2023c; Gruber et al. 2010; Gruber et al. 2012; Kitano et al. 2015; Lai and Chakraborty 2016a, 2016b; Lai et al. 2017a, b, c; Lai et al. 2017a; Lai et al. 2017b; Lai et al. 2018a; Poinsot et al. 1993; Sellmann et al. 2017) means. The advancements in high-performance computing have enabled Direct Numerical Simulations (DNS) of premixed FWI which can provide three-dimensional temporally and spatially resolved data which are either difficult or impossible to obtain using experimental diagnostics. These DNS studies provided important insights into the statistics of wall heat flux (Ahmed et al. 2023a, b; Alshaalan and Rutland 2002; Bruneaux et al. 1996; Bruneaux et al. 1997; Ghai et al. 2023a; Jiang et al. 2019; Lai et al. 2018a; Lai et al. 2022; Poinsot et al. 1993; Zhao et al. 2018a, b), near-wall flow dynamics and species distributions (Ahmed et al. 2018; Ahmed et al. 2019; Ahmed et al. 2021b; Gruber et al. 2010; Gruber et al. 2012; Jiang et al. 2019; Jiang et al. 2021; Kitano et al. 2015; Lai et al. 2017a, b, c; Lai et al. 2017b; Lai et al. 2018a; Zhao et al. 2018a, 2018b, 2021), reactive scalar gradient (Ahmed et al. 2020; Ahmed et al. 2021c; Gruber et al. 2010; Gruber et al. 2012; Konstantinou et al. 2020; Lai and Chakraborty 2016a, 2016b; Lai et al. 2018a; Lai et al. 2022; Sellmann et al. 2017; Zhao et al. 2018b, 2019), flame propagation during turbulent premixed FWI (Ahmed et al. 2020, 2021c; Konstantinou et al. 2020; Lai et al. 2017a; Zhao et al. 2018a, b, 2021) and contributed to the understanding and development of turbulent scalar flux (Ahmed et al. 2021b; Lai et al. 2017a) and mean reaction rate closures (Ahmed et al. 2021a, b, c, d; Ghai et al. 2023b; Lai and Chakraborty 2016a; Lai et al. 2018a; Lai et al. 2022; Sellmann et al. 2017; Zhao et al. 2018a, b) during turbulent premixed FWI. The engineering simulations of FWI using Reynolds Averaged Navier–Stokes (RANS) and hybrid RANS-Large Eddy Simulations (LES) methodologies need highly accurate wall-functions for mean velocity and temperature predictions in turbulent reacting boundary layers. However, the existing wall functions for turbulent boundary layers are proposed for small changes in temperature and density (Durbin and Pettersson Reif 2010; Hanjalić and Launder 2011; Wilcox 1998) but density, viscosity and temperature change significantly within the turbulent boundary layer during FWI. Angelberger et al. (1997) and Han et al. (1996) proposed some modifications to the wall functions of mean velocity and temperature to account for the effects of the changes in thermophysical properties because of the temperature rise within turbulent reacting flow boundary layers. However, to date, limited effort has been directed to the assessment of the performances of the existing (Durbin and Pettersson Reif 2010; Hanjalić and Launder

2011; Wilcox 1998) and modified (Angelberger et al. 1997; Han et al. 1996) wall functions using DNS data of premixed FWI. In this work the performances of wall functions of mean values of streamwise velocity and temperature have been assessed for unsteady head-on quenching (HOQ) of statistically planar flames across turbulent boundary layers for friction Reynolds numbers of $Re_\tau = 110$ and 180. In this respect, the main objectives of the current study are:

(1) To assess the performance of the standard wall functions for mean streamwise velocity and temperature at two different Reynolds numbers.
(2) To provide physical explanations for the statistical behaviours of the performances of the standard wall functions analysed in 1.
(3) To propose modifications to the wall functions of mean streamwise velocity and temperature for FWI, if necessary, and validate them using DNS data.

The rest of the paper is organised as follows. The mathematical background and numerical implementation pertaining to the current analysis are presented in Sects. 2 and 3, respectively. The results are presented and discussed in Sect. 4. The main findings are summarised, and conclusions are drawn in the final section.

2 Mathematical Background

The mean wall shear stress in the viscous sub-layer region of a constant density non-reacting turbulent boundary layer is expressed as $\overline{\tau}_w = \mu(\partial \tilde{u}/\partial y)_w$ (Pope 2000). Here $\tilde{u}$ is the Favre-mean streamwise velocity component, $\overline{\tau}_w$ is the mean wall shear stress, μ is the dynamic viscosity, and $y-$ direction aligns with the wall-normal direction and the streamwise direction is aligned with x. The terms, $\overline{q}, \tilde{q} = \overline{\rho q}/\overline{\rho}$ and $q'' = q - \tilde{q}$ are the Reynolds averaged, Favre-averaged and Favre fluctuations of a general quantity q, respectively and ρ is the gas density. Although density is constant in a boundary layer of a non-reacting incompressible flow, the expressions are still written in terms of Favre averages and $\overline{\rho}$ are used in these expressions because these expressions are often adopted for specifying wall conditions during FWI. The equation representing $\overline{\tau}_w$ leads to:

$$\frac{\tilde{u}}{u_\tau} = \frac{u_\tau y}{v_w} \text{ or } u^+ = y^+ \tag{1}$$

where $u_\tau = \sqrt{|\overline{\tau}_w|/\overline{\rho}_w}$ is the friction velocity, v is the kinematic viscosity and $y^+ = u_\tau y/v_w$ is the normalised wall normal distance y. The subscript 'w' is used to refer to wall values. Equation 1 is valid within the viscous sub-layer (i.e. $y^+ \leq 10.8$) where the viscous effects dominate over the inertial effects (Durbin and Pettersson Reif 2010; Hanjalić and Launder 2011; Pope 2000).

It is important to consider the turbulent kinetic energy transport in order to understand the theoretical framework underpinning the wall functions for velocity in the case of turbulent boundary layers. The transport equation for the Favre averaged turbulent kinetic energy, $\tilde{k} = 0.5\overline{\rho u_i'' u_i''}/\overline{\rho}$ is expressed as follows (Chakraborty et al. 2011a, b; Ghai et al. 2023c; Nishiki et al. 2002):

$$\frac{\partial(\overline{\rho}\tilde{k})}{\partial t} + \frac{\partial(\overline{\rho}\tilde{u}_j\tilde{k})}{\partial x_j} = \underbrace{-\overline{\rho u_i'' u_j''}\frac{\partial \tilde{u}_i}{\partial x_j}}_{P_k} \underbrace{-\overline{u_i''}\frac{\partial \overline{p}}{\partial x_i}}_{P_w} + \underbrace{\overline{p'\frac{\partial u_k''}{\partial x_k}}}_{P_D} - \underbrace{\frac{\partial\left(\overline{p'u_i''}\right)}{\partial x_i}}_{P_T} - \underbrace{\frac{\partial\left(\overline{0.5u_i'' u_k'' u_k''}\right)}{\partial x_i}}_{T_T}$$

$$\underbrace{-\,\overline{\rho}\tilde{\varepsilon}}_{D} + \underbrace{\nabla\cdot\left(\mu\nabla\tilde{k}\right)}_{M_D} + \underbrace{\overline{u_i''\frac{\partial}{\partial x_k}\left(\mu\frac{\partial u_k''}{\partial x_i}\right)} - \frac{2}{3}\overline{u_i''\frac{\partial}{\partial x_i}\left(\mu\frac{\partial u_k''}{\partial x_k}\right)}}_{V} \qquad (2)$$

The terms on the right-hand side of Eq. 2 are as follows: (i) P_k = production term, (ii) P_w = pressure work term, (iii) P_D = pressure dilatation term, (iv) P_T = pressure transport term, (v) T_T = turbulent transport term, (vi) $D = \overline{\mu\left(\partial u_i''/\partial x_j\right)\left(\partial u_i''/\partial x_j\right)}$ = dissipation term where $\tilde{\varepsilon} = D/\overline{\rho}$ is the dissipation rate of turbulent kinetic energy, (vii) M_D = molecular diffusion term, and (viii) V = viscous dissipation term related to dilatation rate.

The equilibrium of the production, P_k, and dissipation, D, in the $\tilde{k}$ transport equation within the inertial layer (i.e. $y^+ \gg 10.8$ and $\mu(\partial\tilde{u}/\partial y) \ll -\overline{\rho u'' v''}$ where v'' is the Favre-fluctuation of the wall normal velocity component) leads to the following relation for a non-reacting constant density boundary layer over a flat plate (Durbin and Pettersson Reif 2010; Hanjalić and Launder 2011; Pope 2000):

$$-\overline{\rho u'' v''}\left(\frac{\partial \tilde{u}}{\partial y}\right) = D \qquad (3)$$

According to Boussinesq's hypothesis $-\overline{\rho u'' v''}$ can be modelled as: $-\overline{\rho u'' v''} = \overline{\rho}v_t(\partial\tilde{u}/\partial y)$ where v_t is the kinematic eddy viscosity. As the inertial layer is assumed to have constant shear stress, this leads to the following expression for constant density non-reacting turbulent boundary layer (Durbin and Pettersson Reif 2010; Hanjalić and Launder 2011; Pope 2000):

$$\overline{\rho}v_t(\partial\tilde{u}/\partial y) = \overline{\tau}_w \text{ or } v_t(\partial\tilde{u}/\partial y) = u_\tau^2 \qquad (4)$$

The inertial range scaling $(\partial\tilde{u}/\partial y) \sim u'/l$ and $v_t \sim u'l$ with u' and l being the root-mean-square turbulent velocity and mixing length scale, respectively, give rise to $u' \sim u_\tau$. For turbulent non-reacting flow boundary layers v_t is found to be: $v_t = \kappa u_\tau y$ where $\kappa = 0.41$ is the von-Karman's constant (Durbin and Pettersson Reif 2010; Hanjalić and Launder 2011; Pope 2000). This leads to $\tilde{\varepsilon} = u_\tau^3/(\kappa y)$ in the inertial layer and using this relation in Eq. 3 yields:

$$u^+ = \frac{\tilde{u}}{u_\tau} = \frac{1}{\kappa}\ln y^+ + \underbrace{C_1 - \frac{1}{\kappa}\ln\frac{u_\tau}{v}}_{B} = \frac{1}{\kappa}\ln y^+ + B \qquad (5)$$

In Eq. 5, B depends on Reynolds number but assumes a value ranging from 5.0 to 6.5 (Durbin and Pettersson Reif 2010; Pope 2000; Wilcox 1998).

Similarly, in the corresponding turbulent thermal boundary layer, the following expression is obtained for the mean wall heat flux $\overline{q}_w$:

$$\bar{q}_w = -\lambda \left.\frac{\partial \tilde{T}}{\partial y}\right|_w - \overline{\rho v'' T''} \tag{6}$$

where λ is the thermal conductivity. For an isothermal wall, a non-dimensional temperature can be defined as (Hanjalić and Launder 2011; Kays and Crawford 1993):

$$T^+ = \frac{\rho_w c_p u_\tau \left(T_w - \tilde{T}\right)}{\bar{q}_w} \tag{7}$$

where T_w is the wall temperature. Using Eq. 7 and the gradient hypothesis closure for the Reynolds flux of temperature $-\overline{\rho v'' T''} = \left(\bar{\rho} v_t / Pr_t\right)(\partial \tilde{T}/\partial y)$ yields (Hanjalić and Launder 2011; Kays and Crawford 1993):

$$\left(\frac{1}{Pr} + \frac{v_t}{v}\frac{1}{Pr_t}\right)\frac{\partial T^+}{\partial y^+} = 1.0 \tag{8}$$

Equation 8, in turn, leads to (Hanjalić and Launder 2011; Kays and Crawford 1993):

$$T^+ = \int_0^{y^+} \frac{dy'^+}{\left(\frac{1}{Pr} + \frac{v_t}{v}\frac{1}{Pr_t}\right)} \tag{9}$$

In order to evaluate Eq. 9, the combination of Eqs. 1 and 4 provides (Hanjalić and Launder 2011; Kays and Crawford 1993):

$$u^+ = \int_0^{y^+} \frac{dy'^+}{\left(1 + \frac{v_t}{v}\right)} \tag{10}$$

A combination of Eqs.9 and 10 gives rise to:

$$T^+ = Pr_t u^+ + B_c\left(Pr, Pr_t\right) \tag{11}$$

where $B_c\left(Pr, Pr_t\right)$ is given by:

$$B_c\left(Pr, Pr_t\right) = \int_0^{y^+} \frac{Pr_t \, dy'^+}{\left(\frac{Pr_t}{Pr} + \frac{v_t}{v}\right)} - \int_0^{y^+} \frac{Pr_t \, dy'^+}{\left(1 + \frac{v_t}{v}\right)} \tag{12}$$

In the viscous-sublayer (i.e. $y^+ \leq 10.8$), Eq. 1 can be used in Eq. 11 to yield (Hanjalić and Launder 2011; Kays and Crawford 1993):

$$T^+ = Pr y^+ \tag{13}$$

whereas in the inertial sub-layer (i.e. $y^+ > 10.8$), the following expression is obtained (Hanjalić and Launder 2011; Kays and Crawford 1993):

$$T^+ = \frac{Pr_t}{\kappa}\ln y^+ + Pr_t B + B_c\left(Pr, Pr_t\right) \tag{14}$$

Equation 14 has been approximated by Kays and Crawford (1993) as:

$$T^+ = 2.075 \ln y^+ + 3.9 \tag{15}$$

The relations given by Eqs. 1,5, 13, 14 and 15 were derived for non-reacting constant density flows and they have been applied successfully for heat transfer problems where the temperature change is not large enough to change density and kinematic viscosity by an order of magnitude. However, these relations may not be valid in the presence of significant changes in density and kinematic viscosity during FWI.

To account for changes in density and kinematic viscosity there are a number of different transformations available in the literature for velocity and wall distance in the case of compressible or variable density flows and all these transformations can be cast in terms of the mapping functions S_1 and S_2 for wall normal distance and mean velocity defined as:

$$\eta^+ = \int_0^{y^+} S_1 dy^+ \quad \text{and} \quad \psi^+ = \int_0^{u^+} S_2 du^+ \tag{16}$$

The summary of the different proposed transformations can be found in Table 1. To satisfy the inner layer similarly, mapping functions must satisfy this relation, $S_1 = S_2/(G \times H)$ (Volpiani et al. 2020). The above relation can be derived either by enforcing universality of the viscous sublayer or by enforcing universality in the Morkovin-scaled Reynolds shear stress throughout the inner layer. The transformations that satisfy the above relation can predict reasonable results until the edge of the viscous sublayer. Only few transformations that are listed in Table 1 can satisfy this relation (Angelberger et al. 1997; Han et al. 1996; Trettel and Larsson 2016; Volpiani et al. 2020). However, for non-adiabatic turbulent boundary layer flows, the transformations proposed by Angelberger et al. (1997) and Han et al. (1996) provide reasonable results within the whole domain and these wall functions were proposed in the context of FWI. Therefore, in this work modifications have been suggested to the transformation given by Angelberger et al. (1997) and Han et al. (1996) to account for changes in density and kinematic viscosity in the reacting flow boundary layer. The interested readers are referred to Sect. 4 of this paper for further information in this regard. However, the predictions of other transformations (Howarth and Taylor 1997; Trettel and Larsson 2016; Van Driest 1951; Volpiani et al. 2020) are also shown in the Appendix A of this paper for the sake of completeness.

Angelberger et al. (1997) and Han et al. (1996) proposed empirical modifications to the laws of the wall (i.e., Eqs. 1, 5, 13, 15) using following transformations:

Table 1 Transformation for wall normal distance and mean velocity according to Eq. 16 with $G = \overline{\rho}/\overline{\rho}_w$ and $H = \tilde{v}/v_w$

Transformations	S_1	S_2
Viscous sublayer	$S_1 = 1$	$S_2 = H \times G$
Van Driest (1951)	$S_1 = 1$	$S_2 = G^{1/2}$
Trettel and Larsson (2016)	$S_1 = \frac{d}{dy}\left(\frac{y}{G^{1/2} \times H}\right)$	$S_2 = (H \times G)\frac{d}{dy}\left(\frac{y}{G^{1/2} \times H}\right)$
Volpiani et al. (2020)	$S_1 = \frac{1}{G \times H^{3/2}}$	$S_2 = 1/H^{1/2}$
Howarth and Taylor (1997)	$S_1 = 1/H^{1/2}$	$S_2 = 1$
Angelberger et al. (1997) and Han et al. (1996)	$S_1 = 1/H$	$S_2 = G$

$$d\eta^+ = \frac{\nu_w}{\tilde{\nu}}dy^+; \ \ d\psi^+ = \frac{\overline{\rho}}{\rho_w}du^+ \ \text{and} \ d\Theta^+ = \frac{\overline{\rho}}{\rho_w}dT^+ \tag{17}$$

Based on Eq. 17, the kinematic viscosity compensated non-dimensional wall normal distance η^+ at a location corresponding to y_1^+ is approximated as (Angelberger et al. 1997; Han et al. 1996; Poinsot and Veynante 2005):

$$\eta^+ = \int_0^{y_1^+} \frac{\nu_w}{\tilde{\nu}}dy^+ \approx \frac{\nu_w}{\tilde{\nu}}y_1^+ \tag{18}$$

Similarly, the density compensated non-dimensional streamwise velocity ψ^+ corresponding to $u_1^+ = u^+\left(y_1^+\right)$ is approximated as (Angelberger et al. 1997; Han et al. 1996; Poinsot and Veynante 2005):

$$\psi^+ = \int_0^{u_1^+} \frac{\overline{\rho}}{\rho_w}du^+ \approx \frac{\overline{\rho}u_1^+}{\rho_w} \tag{19}$$

Using $\tilde{T} = T_w\left(1 + \xi T^+\right)$ with ξ being $\xi = -\overline{q}_w/\left(\rho_w c_p u_\tau T_w\right)$ allows for expressing the mean density as $\overline{\rho}/\rho_w = 1/\left(1 + \xi T^+\right)$ for constant pressure, which upon using in Eq. 17 yields (Angelberger et al. 1997; Han et al. 1996; Poinsot and Veynante 2005):

$$\Theta^+ = \int_0^{T^+} \frac{dT'^+}{\left(1 + \xi T'^+\right)} = \frac{\ln\left(1 + \xi T^+\right)}{\xi} = \frac{1}{\xi}\ln\left(\frac{\tilde{T}}{T_w}\right) \tag{20}$$

According to Angelberger et al. (1997) and Han et al. (1996) y^+, u^+ and T^+ in Eqs. 1, 5, 13 and 15 are substituted by η^+, ψ^+ and Θ^+, respectively to obtain revised 'laws of the wall' in the following manner (Poinsot and Veynante 2005):

$$\psi^+ = \eta^+ \ \text{and} \ \Theta^+ = Pr\eta^+ \ \text{for} \ \eta^+ \leq 10.8 \tag{21}$$

$$\psi^+ = \frac{1}{\kappa}\ln\eta^+ + B \ \text{and} \ \Theta^+ = 2.075\ln\eta^+ + 3.9 \ \text{for} \ \eta^+ > 10.8 \tag{22}$$

However, it is worthwhile to note that the success of Eqs. 21 and 22 also depends on the modelled expressions of η^+ and ψ^+ given by Eqs. 18 and 19, respectively. The applicability of Eqs. 1, 5, 13, 15, 18, 19, 21 and 22 during FWI in turbulent boundary layers will be assessed in Sect. 4 of this paper.

3 Numerical Implementation

In this work, DNS databases of unsteady HOQ of statistically planar flames across turbulent boundary layers due to interaction with isothermal inert walls have been considered for friction velocity-based Reynolds numbers Re_τ of 110 and 180. In the existing literature, the friction velocity Re_τ of 180 is often regarded as a benchmark case for DNS of fully developed turbulent channel flows (Kawamura et al. 1998; Kim et al. 1987) because all the

turbulence statistics for this friction Reynolds number is qualitatively similar to those for higher values of Re_τ (Kawamura et al. 1998; Kim et al. 1987) but can be afforded without exorbitant computational cost. It is worth noting that turbulent boundary layers in internal combustion engines are characteristic of low Re_τ values (e.g., Re_τ ranging from 100 to 200). Therefore, Re_τ of 110 is considered in this analysis to ensure that the findings for $Re_\tau = 180$ also remain valid for weakly turbulent boundary layers. Moreover, the computational requirement of the DNS considered here, with a maximum mesh size of 1.536 billion, also played a crucial role in determining the Reynolds numbers. Higher Reynolds numbers demand finer meshes and thus are more computationally expensive. Thus, the chosen Re_τ values are deemed appropriate to ensure a reasonable compromise between computational cost and required physical insights within the constraints of available computational resources.

The simulations have been conducted using a compressible DNS code SENGA + (Jenkins and Cant 1999), which solves conservation equations of mass, momentum, energy and species in non-dimensional form. In SENGA+, spatial derivatives for internal grid points are systematically computed utilising a 10th-order central difference scheme. However, it is noteworthy that the order of accuracy gradually diminishes to a one-sided 2nd-order scheme at the non-periodic boundaries, as explained by Jenkins and Cant (1999). Temporal progression in these simulations is achieved through the utilisation of a low storage explicit 3rd-order Runge–Kutta scheme.

A generic single step irreversible chemical reaction representing fuel and oxidiser is considered in the present work: 1 unit mass of Fuel + s unit mass of Oxidiser → (1 + s) unit mass of Products, where s is the stoichiometric oxidiser-fuel mass ratio. Here, fuel is methane CH_4, oxidiser is O_2 and products is CO_2 and N_2 in the air is considered to be inert. This yields a value of $s = 4.0$ for methane-air combustion. The reactants of the stoichiometric methane-air mixture in their unburned state undergo preheating to a temperature of 730 K. This preheating condition results in the determination of the heat release parameter τ, expressed as the ratio $(T_{ad} - T_0)/T_0$, where T_0 denotes the unburned gas temperature, and T_{ad} represents the adiabatic flame temperature. Specifically, in this scenario, the calculated value for τ is 2.3. It is pertinent to note that standard values are employed for the Prandtl number Pr and the ratio of specific heats γ, with Pr assigned a value of 0.7 and γ set at 1.4. The Lewis number Le of all the species are taken to be unity for the sake of simplicity as the fuel and oxidiser for the present analysis (i.e. methane and oxygen) have Lewis numbers close to unity (= 0.96 and 1.10 for methane and oxygen, respectively) (Smooke and Giovangigli 1991). It is important to note that the present analysis focuses principally on the statistics related to turbulent fluid motion, which are only affected by the density change and dilatation rate arising from chemical heat release. Thus, the exact nature of chemical mechanism is not expected to have a major impact on the statistics presented here. Moreover, it has been demonstrated elsewhere (Ahmed et al. 2018, 2021b; Lai et al. 2022; Zhao et al. 2018a, b) that the statistics of vorticity, reactive scalar gradient, maximum wall heat flux magnitude and the flame quenching distance obtained from single step chemistry (Ahmed et al. 2018; Ahmed et al. 2021c; Lai and Chakraborty 2016a; Lai et al. 2018a; Poinsot et al. 1993; Sellmann et al. 2017) are in good qualitative and quantitative agreement with the corresponding detailed chemistry results (Ahmed et al. 2018; Ahmed et al. 2021b; Lai et al. 2018a; Lai et al. 2022). Thus, it can be expected that the findings of the current analysis will be at least qualitatively valid in the presence of detailed chemistry. The aforementioned studies, encompassing both single-step irreversible chemical reactions representing fuel and oxidiser, as well as those employing detailed chemistry, serve as

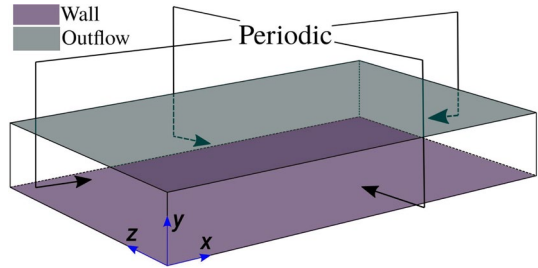**Fig. 1** Schematic diagram of the HOQ configuration

Table 2 Simulation parameters for the HOQ configuration for $Re_\tau = 110$ and 180

Parameters	$Re_\tau = 110$	$Re_\tau = 180$
Computational domain size $(L_x \times L_y \times L_z)$	$10.69h \times 1.33h \times 4h$	$10.69h \times 1.33h \times 4h$
Grid resolution	$1920 \times 240 \times 720$	$3200 \times 400 \times 1200$

representations of stoichiometric methane-air (Ahmed et al. 2018, 2021b; Lai et al. 2018a) and stoichiometric hydrogen-air (Lai et al. 2022) mixtures.

The bulk Reynolds number for the non-reacting fully developed channel flow simulations which are used to initilise the reacting flow simulations are $Re_b = 2\rho_0 u_b h/\mu_0 = 3285$ and 5665 for $Re_\tau = 110$ and 180, respectively where $u_b = 1/2h \int_0^{2h} u\,dy$ is the bulk mean velocity, ρ_0 is the unburned gas density, h is the half channel height, and μ_0 is the unburned gas viscosity. The ratio of unstretched laminar burning velocity to the non-reacting flow friction velocity, denoted as $S_L/u_{\tau,NR}$, is taken to be 0.7. The Mach number based on $u_{\tau,NR}$, represented as $Ma = u_{\tau,NR}/a_0$ (where a_0 is the acoustic speed in the unburned gas), is 3×10^{-3} for all cases considered. Validation of the non-reacting flow simulation results has been undertaken by comparing them to prior research findings, specifically those presented by Tsukahara et al. (2005). The achieved agreement, as reported in studies by Ahmed et al. (2021a, 2021b, 2021c, 2021d), attests to the reliability and accuracy of the simulations in capturing the fundamental flow features. For these simulations, key parameters such as the longitudinal integral length scale L_{11} and the root-mean-square velocity fluctuation exhibit scaling relationships with h and $u_{\tau,NR}$ respectively, as shown by Ahmed et al. (2021a), which yield a Damköhler number $Da = L_{11}S_L/u'\delta_{th}$ of 15.80 and 26, and a Karlovitz number $Ka = (u'/S_L)^{3/2}(L_{11}/\delta_{th})^{-1/2}$ of 0.36 and 0.28 for Re_τ of 110 and 180, respectively. These values are representative of the corrugated flamelets regime combustion when the flame is away from the wall (Peters 2000).

The schematic diagram for the HOQ configuration is shown in Fig. 1. The computational domain size and the corresponding grid size are listed in Table 2 for the cases considered in the present work. The grid resolution employed in these simulations guarantees a minimum of 8 grid points within the thermal flame thickness, denoted as $\delta_{th} = (T_{ad} - T_0)/\max|\nabla T|_L$, where T represents the instantaneous temperature. Additionally, a stringent criterion is imposed to maintain a maximum value of y^+ (dimensionless distance from the wall) not exceeding 0.6 for the grid points adjacent to the wall. Periodic boundary conditions are specified for the streamwise ($x-$direction) and spanwise ($z-$direction) dimensions, while the mean pressure gradient, expressed as $-\partial\overline{p}/\partial x = \overline{\rho}u_{\tau,NR}^2/h$

(where p denotes pressure), is applied in the streamwise flow direction. A no-slip boundary condition is implemented at $y = 0$, and the wall temperature T_w is equal to the unburned gas temperature T_0, which is specified, $T_w = T_0 = 730K$ as isothermal wall boundary condition. The wall-normal mass flux is constrained to zero at the wall. At $y/h = 1.33$, a partially non-reflecting boundary is prescribed based on the NSCBC conditions proposed by Yoo and Im (2007). Initialisation of the reacting flow field is carried out such that the reaction progress variable, denoted as c, attains a value of 0.5 at $y/h \approx 0.85$. In this context, the reaction progress variable c is defined in terms of the fuel mass fraction Y_F, given by $c = (Y_{FR} - Y_F)/(Y_{FR} - Y_{FP})$ where subscripts R and P represent the fresh reactant and fully burned products, respectively. This formulation ensures that c ranges from 0.0 in the unburned gas to 1.0 in the fully burned gas. The initialisation of the reacting scalar field is designed such that the reactant side of the flame faces the wall, while the product side of the flame consistently orients towards the outflow side of the boundary in the y−direction. The simulation duration spans a maximum of 2.0 flow-through times, corresponding to $21.30t_f$ and $30.3t_f$ for Re_τ values of 110 and 180, respectively, where t_f is the chemical timescale, defined as $t_f = \delta_{th}/S_L$. During the simulation period, the flame propagates towards the wall and interacts with it, although the boundary layer exhibits minimal evolution, as corroborated by the corresponding non-reacting flow simulation (Ahmed et al. 2021a, 2021b, 2021c, 2021d). The Reynolds and Favre averaged quantities, involving correlations of Reynolds and Favre fluctuations in the HOQ configuration under consideration, are determined by spatial averaging the relevant parameters within the periodic directions (i.e., $x - z$ planes) at a given time instant.

4 Results and Discussion

4.1 Instantaneous and Mean Scalar Fields

The isosurfaces of reaction progress variable $c = 0.8$ at the different stages of HOQ (i.e., for different values of t/t_f) of the statistically planar flame are shown in Fig. 2a, b at $t/t_f = 3.99, 10.92, 13.12, 16.27$ for $Re_\tau = 110$ and at $t/t_f = 7.89, 14.38, 16.75, 20.11$ for 180, respectively along with the distributions of normalised vorticity magnitude $\Omega = \sqrt{w_i w_i} \times h/u_{\tau,NR}$ on the $x - y$ plane at $z/h = 4$, where w_i is the *ith* component of vorticity. The aforementioned time instants with increasing values of t/t_f correspond to the normalised wall normal distance of $y/h = 0.72, 0.22, 0.06$ and 0.03 of non-dimensional temperature $\tilde{\theta} = (\tilde{T} - T_0)/(T_{ad} - T_0) = 0.5$ isosurface, respectively for both values of Re_τ. The vortical flow structures close to the wall, as can be seen from Fig. 2a, b, affect the flame wrinkling and the interaction of the flame surface with the wall leads to eventual flame quenching due to heat loss through the cold isothermal wall. The effect of the increase in the Re_τ is reflected in the higher extent of wrinkling of the $c = 0.8$ isosurface in Fig. 2b than in Fig. 2a. At higher Re_τ values, the flame wrinkling increases due to stronger turbulent activity within the boundary layer, which is reflected in the higher magnitudes of turbulent burning velocity $S_T = \int \dot{\omega}_c dV/\rho_0 A_p$ (where A_p is the projected flame area in the direction of mean flame propagation, $\dot{\omega}_c$ is the reaction rate of progress variable and ρ_o is the unburnt gas density) for a given wall-normal distance of $\tilde{\theta} = 0.5$ isosurfaces in the $Re_\tau = 180$ case than in the $Re_\tau = 110$ case, which can be substantiated from the Table 3.
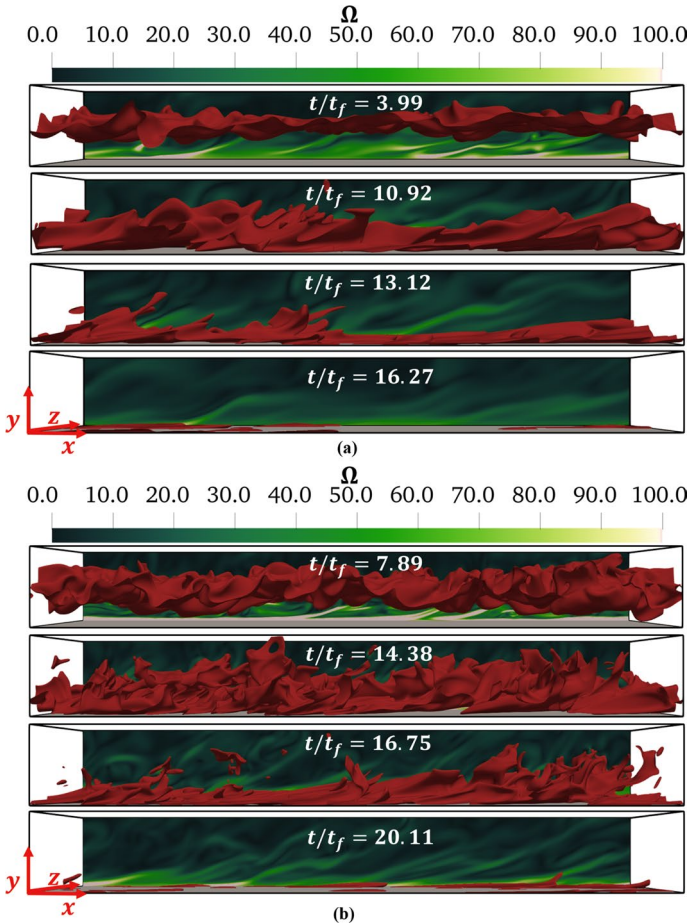
Fig. 2 Isosurfaces of reaction progress variable $c = 0.8$ at the different stages of HOQ of the statistically planar flame in terms of t/t_f at (**a**) $Re_\tau = 110$ and (**b**) $Re_\tau = 180$. The distributions of normalised vorticity magnitude $\Omega = \sqrt{w_i w_i} \times h/u_{\tau,NR}$ is shown on the $x - y$ plane at $z/h = 4$

Table 3 The values of the normalised turbulent burning velocity S_T/S_L for the $Re_\tau = 110$ and 180 case of HOQ configuration at different t/t_f and $y_{\bar{\theta}=0.5}/h$.	$Re_\tau = 110$ and 180	$Re_\tau = 110$		$Re_\tau = 180$	
	$y_{\bar{\theta}=0.5}/h$	t/t_f	S_T/S_L	t/t_f	S_T/S_L
	0.72	3.99	1.005	7.89	1.580
	0.22	10.92	1.312	14.38	1.970
	0.06	13.12	0.563	16.75	0.849
	0.03	16.27	0.028	20.11	0.047

Therefore, the interaction between flame and wall surface becomes stronger for higher values of Re_τ where the flame elements are convected more strongly towards the wall by the turbulent fluid motion.

In the case of low Mach number globally adiabatic premixed flames, $c = \theta$ (where $\theta = (T - T_0)/(T_{ad} - T_0)$ is the non-dimensional temperature) is maintained without any significant heat loss but the requirements of $c = \theta$ are not met in the vicinity of an isothermal wall boundary condition. The instantaneous distributions of $(c - \theta)$ at the central midplane for both cases are shown in Fig. 3. Initially, away from the wall, there is a coherent maintenance of the relationship $c = \theta$, indicating a coupling between progress variable, c and non-dimensional temperature θ. However, in close proximity to the wall, a pronounced decoupling between c and θ is evident. This decoupling originates due to the imposed boundary conditions at the wall. The non-dimensional temperature θ at the wall is maintained to a constant value of 0.0 due to an imposed isothermal wall boundary condition. By contrast, the progress variable c undergoes an increase from 0.0 as the flame quenching progresses due to the zero wall normal gradient boundary condition. This increase in c is attributed to the diffusion of unburned gas from the vicinity of the wall towards the interior of the domain. Therefore, the value of $(c - \theta)$ emerges as a distinctive marker of FWI, providing valuable insights into the progress of flame quenching. (Ahmed et al. 2021a, b, c, d; Ahmed et al. 2023a, b; Ghai et al. 2022a, b, c). This can be substantiated from Fig. 4, which shows that the evolutions of $(\tilde{c}_w - \tilde{\theta}_w)$ (where the subscript w is used for wall values) and the mean normalised wall heat flux magnitude $\overline{\Phi} = |\overline{q}_w|/[\rho_0 c_{p0} S_L (T_{ad} - T_0)]$ with normalised time t/t_f, where c_{p0} and q_w are the specific heat at constant pressure in the unburned gas, and wall heat flux respectively. It can be seen from Fig. 4 that $(\tilde{c}_w - \tilde{\theta}_w)$ starts to assume significant non-zero values when $\overline{\Phi}$ takes non-zero values, which can be considered as the marker of the initiation of FWI. The magnitude of $\overline{\Phi}$ starts to drop once the flame is quenched but $(\tilde{c}_w - \tilde{\theta}_w)$ continues to increase until it assumes a value of 1.0. The normalised maximum heat flux magnitude $\Phi_{max} = |q_w|_{max}/[\rho_0 c_{p0} S_L (T_{ad} - T_0)]$, minimum Peclet number $Pe_{min} = \delta_Q/\delta_z$ (i.e. the minimum wall normal distance δ_Q of the $\theta = 0.75$ isosurface normalised by the
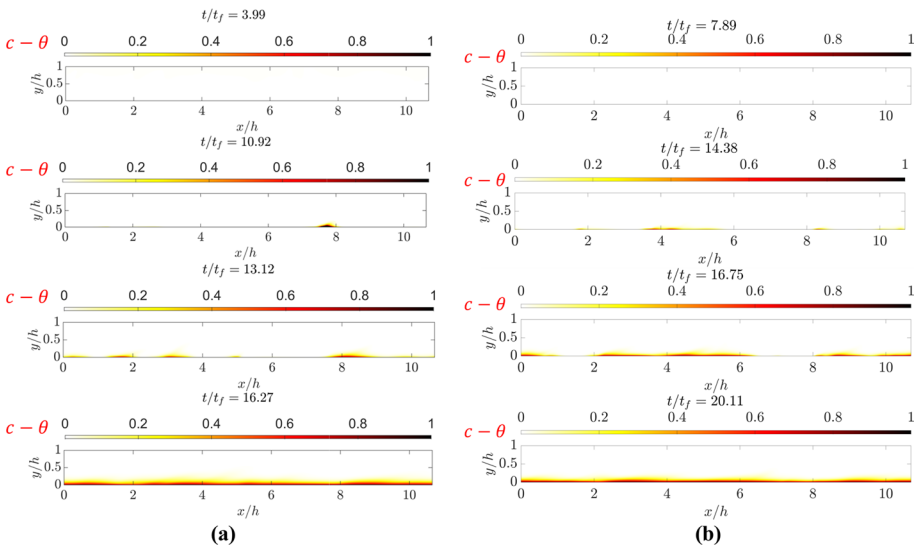

Fig. 3 Instantaneous distributions of $(c - \theta)$ is shown in the central midplane at the different stages of HOQ (i.e. for different values of t/t_f) of the statistically planar flame for (a) $Re_\tau = 110$ and (b) $Re_\tau = 180$
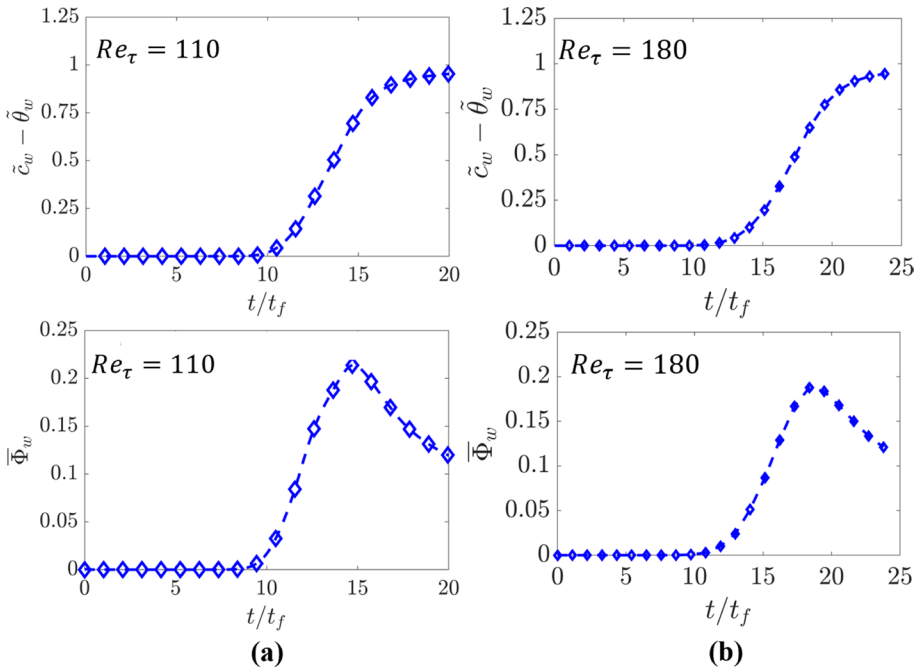
Fig. 4 Distributions of $(\tilde{c}_w - \tilde{\theta}_w)$ (1st row) and the mean normalised wall heat flux magnitude $\overline{\Phi} = |\overline{q}_w| / [\rho_0 c_{p0} S_L (T_{ad} - T_0)]$ (2nd row) with normalised time t/t_f for statistical planar flame HOQ case for (**a**) $Re_\tau = 110$ and (**b**) $Re_\tau = 180$

Zel'dovich flame thickness $\delta_z = \alpha_{T0}/S_L$ with α_{T0} being the thermal diffusivity in the unburned gas) are often used to characterise the FWI process. Note that the maximum heat release rate in the unstretched freely propagating laminar premixed flame occurs at $\theta = 0.75$ for the present thermochemistry. The Φ_{max} and Pe_{min} values for this turbulent boundary layer HOQ case are 0.47 and 1.71 for $Re_\tau = 110$ and 0.46 and 1.72 for $Re_\tau = 180$. The distributions of Φ and normalised vorticity magnitude Ω on the wall when the minimum Peclet number is observed are shown in Fig. 5a, b, for $Re_\tau = 110$ and 180, respectively, which show the signatures of heat flux streaks induced by vortical motions. The occurrence of heat flux streaks is intimately connected to the dynamic behaviour of vortical structures within the turbulent boundary layer. Vortical motions, characterised by the presence of coherent structures, play a pivotal role in the heat transfer to the wall (Ghai et al. 2023a).

It is not only the wall heat flux but also the wall shear stress τ_w which is affected during FWI. Figure 6 shows the variations of $\overline{\tau}_w/\overline{\tau}_{w,NR}$ and $\overline{u}_\tau/\overline{u}_{\tau,NR} = \sqrt{|\overline{\tau}_w|/\overline{\rho}_w}/\overline{u}_{\tau,NR}$ with the normalised time t/t_f for the statistical planar flame HOQ case, where $\overline{\tau}_w$ is the mean wall shear stress and the subscript NR is used for the corresponding non-reacting values for $Re_\tau = 110$ and 180. The gas density drops with an increase in temperature as the thermodynamic pressure remains almost constant in the cases considered here. Accordingly, density increases as the cold wall is approached and at the wall the density becomes comparable to the unburned gas density (i.e. $\rho_w \approx \rho_0$). In this configuration, the mean direction of flame propagation is perpendicularly aligned with the wall and thus the thermal expansion effects are mostly felt in the wall-normal direction. The
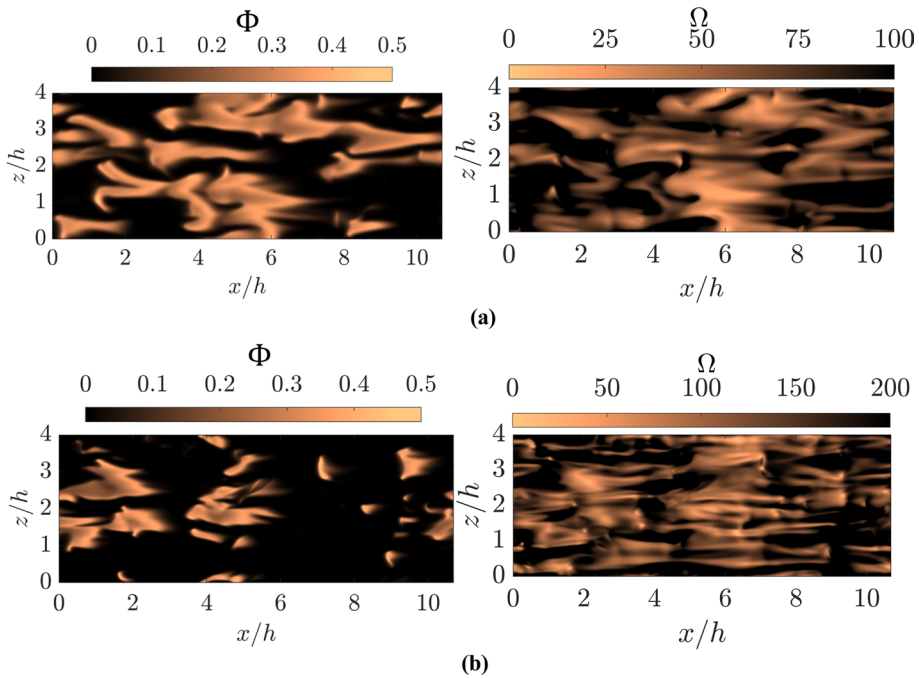
Fig. 5 Instantaneous distributions of Φ (left) and normalised vorticity magnitude Ω (right) on the wall at the time when the maximum heat flux magnitude is obtained for HOQ of statistically planar flame for **(a)** $Re_\tau = 110$ and **(b)** $Re_\tau = 180$

redistribution of momentum due to thermal expansion leads to reductions in $(\partial u/\partial y)_{y=0}$ and τ_w during FWI in the HOQ configuration considered here (Ahmed et al. 2023a, b). This leads to a drop in u_τ during FWI in comparison to the non-reacting channel flow value for the cases considered here (Ahmed et al. 2023a, b). Figures 4 and 6 indicate that both $\overline{q}_w$ and $\overline{\tau}_w$ change during FWI, which, in turn, can affect T^+, u^+ and y^+ values. Therefore, the values of y^+ at a given value of y/h can be different during FWI in both cases considered here.

4.2 Evaluation of Existing Wall Functions

Figure 7 represents the variation of y^+ with y/h and it can be seen from Fig. 7a, b that the range of y^+ values within the region given by $0 < y/h < 1.0$ changes with time. The dynamic changes in y^+ values are indicative of the evolving flow conditions near the wall during FWI. The wall shear stress changes with the progress of FWI in this configuration due to the redistribution of momentum in the near-wall region because of flame normal acceleration indued by thermal expansion, which was discussed in detail by Ahmed et al. (2023a, b) and thus is not repeated here. The time-dependent variation in y^+ values in the unsteady head-on quenching across turbulent boundary layers underscore the need for a nuanced understanding of turbulent boundary layer dynamics during FWI. Moreover, it suggests that wall functions for FWI need to capture the dynamic nature of the near-wall flow dynamics. Furthermore, this has a major implication on the applicability of Eqs. 1, 5,
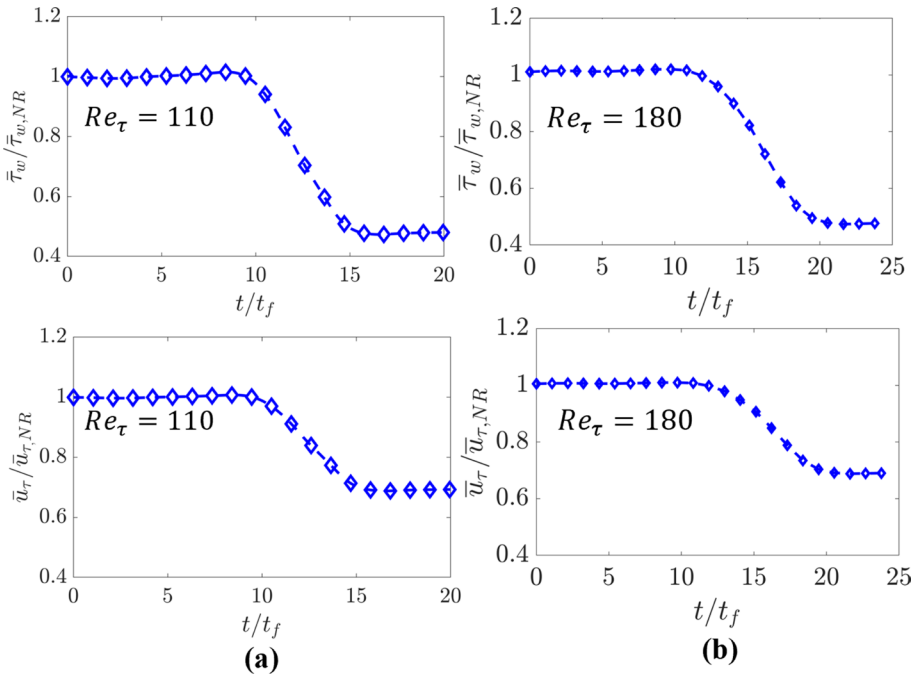
Fig. 6 Variations of $\overline{\tau}_w/\overline{\tau}_{w,NR}$ (1st row) and $\overline{u}_\tau/\overline{u}_{\tau,NR} = \sqrt{|\overline{\tau}_w|/\rho_w}/\overline{u}_{\tau,NR}$ (2nd row) with normalised time t/t_f for statistical planar flame HOQ case for (**a**) $Re_\tau = 110$ and (**b**) $Re_\tau = 180$

13 and 15 within turbulent boundary layers during FWI. Figure 8 shows the variations of normalised Favre mean streamwise velocity u^+ and normalised mean temperature T^+ with normalised wall-normal distance y^+. The variation of u^+ with y^+ in a non-reacting channel flow corresponding to $Re_\tau = 110$ and 180 are also shown in Fig. 8 and it is found that the predictions of Eqs. 1 and 5 agree well with DNS data and the observed variation of u^+ with y^+ is consistent with previous findings (Tsukahara et al. 2005). In Fig. 8, the time instants for the simulations are chosen in such a manner that it ranges from the time when the flame is away from the wall (i.e., $t/t_f < 8.0$) to when it interacts with the wall (i.e., $t/t_f > 10.0$). The predictions of the standard relations for viscous sub-layer (i.e. Equation 2 for $y^+ < 10.8$) and inertial layer (i.e. Equation 5 for $y^+ > 10.8$) are also compared with the variation of u^+ with y^+ extracted from DNS data in Fig. 8 where the predictions of the temperature wall functions for viscous sublayer (i.e. Equation 13) and inertial layer (i.e. Equation 15) are also shown. Figure 8 shows that the variation of u^+ with y^+ from DNS matches reasonably well with $u^+ = y^+$ for $y^+ < 10.8$ for both Re_τ cases, but the agreement with log-law remains unsatisfactory for $y^+ > 10.8$, and the disagreement increases with increasing t/t_f. Moreover, Eqs. 13 and 15 do not capture the variation of T^+ both in the viscous sub-layer and inertial layers.

It is worth noting that Eqs. 1 and 5 assume that $\mu(\partial\tilde{u}/\partial y) - \overline{\rho u''v''}$ remain unchanged and is equal to $\overline{\tau}_w$ in the wall normal direction. The variations of $\mu(\partial\tilde{u}/\partial y)/\overline{\tau}_w, -\overline{\rho u''v''}/\overline{\tau}_w$ and $\left[\mu(\partial\tilde{u}/\partial y) - \overline{\rho u''v''}\right]/\overline{\tau}_w$ with y/h at different time instants for the HOQ of the statistically planar flame are shown in Fig. 9. It can be seen from Fig. 9 that $\mu(\partial\tilde{u}/\partial y)_w = \overline{\tau}_w$ is maintained at the wall because $\overline{\rho u''v''}$ vanishes at the wall, whereas the magnitude of the
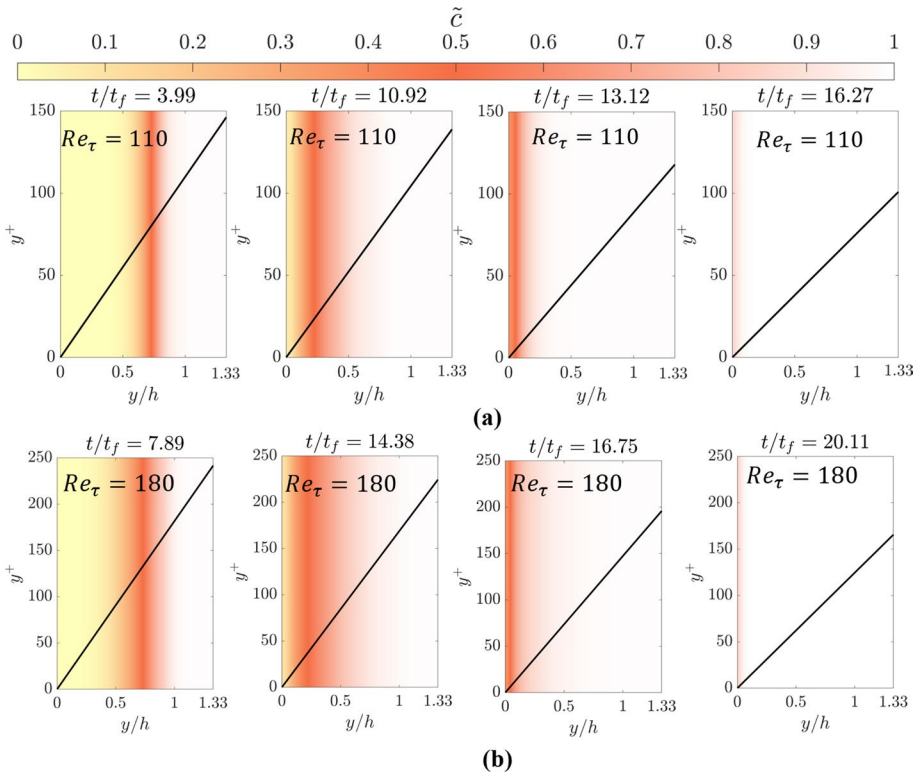
Fig. 7 Variations of y^+ with y/h at different normalised time instants t/t_f for the statistical planar flame HOQ case for (**a**) $Re_\tau = 110$ and (**b**) $Re_\tau = 180$. The background colour in Figs. 6, 7, 8, 9, 10, 11, 12, 13 provides the value of $\tilde{c}$

contribution of $\left(-\overline{\rho u'' v''} \right)$ increases in the wall normal direction. However, the net contribution of $\left[\mu(\partial \tilde{u}/\partial y) - \overline{\rho u'' v''} \right]$ does not remain equal to $\overline{\tau}_w$ but remains always smaller than $\overline{\tau}_w$ away from the wall for both cases. Therefore, the assumption $\left[\mu(\partial \tilde{u}/\partial y) - \overline{\rho u'' v''} \right] = \overline{\tau}_w$ that underpins Eq. 4 is rendered invalid in the reacting flow turbulent boundary layers considered in the current analysis. Moreover, the equilibrium between $P_k = -\overline{\rho u_i'' u_j''} \left(\partial \tilde{u}_i/\partial x_j \right)$ and $\overline{\rho} \tilde{\varepsilon}$ is invoked while deriving the log-law (i.e., Eq. 5) in the inertial layer. The ratio of $P_k / \overline{\rho} \tilde{\varepsilon}$ in the wall-normal distance y/h at different time instants for the HOQ of the statistically planar flame are shown in Fig. 10. Figure 10 further shows that $P_k / \overline{\rho} \tilde{\varepsilon}$ assumes locally negative values for $y^+ > 10.8$ in the HOQ of statistically planar flame. According to the Boussinesq hypothesis, $-\overline{\rho u'' v''}$ can be modelled as: $-\overline{\rho u'' v''} = \overline{\rho} \nu_t (\partial \tilde{u}/\partial y)$, which leads to $P_k = -\overline{\rho u'' v''}(\partial \tilde{u}/\partial y) = \overline{\rho} \nu_t (\partial \tilde{u}/\partial y)^2$ for boundary layer flows considered here. This suggests that $P_k / \overline{\rho} \tilde{\varepsilon}$ becomes equal to $P_k / \overline{\rho} \tilde{\varepsilon} = \nu_t (\partial \tilde{u}/\partial y)^2 / \tilde{\varepsilon}$, which is a positive value. However, negative values of $P_k / \overline{\rho} \tilde{\varepsilon}$ in the region of the flame brush where the effects of heat release rate are strong, shown in Fig. 10, suggests that the Boussinesq hypothesis might not even be qualitatively valid within the flame brush. Figure 10 further shows that $P_k / \overline{\rho} \tilde{\varepsilon}$ assumes positive values in the unburned and burned gases where the thermal expansion
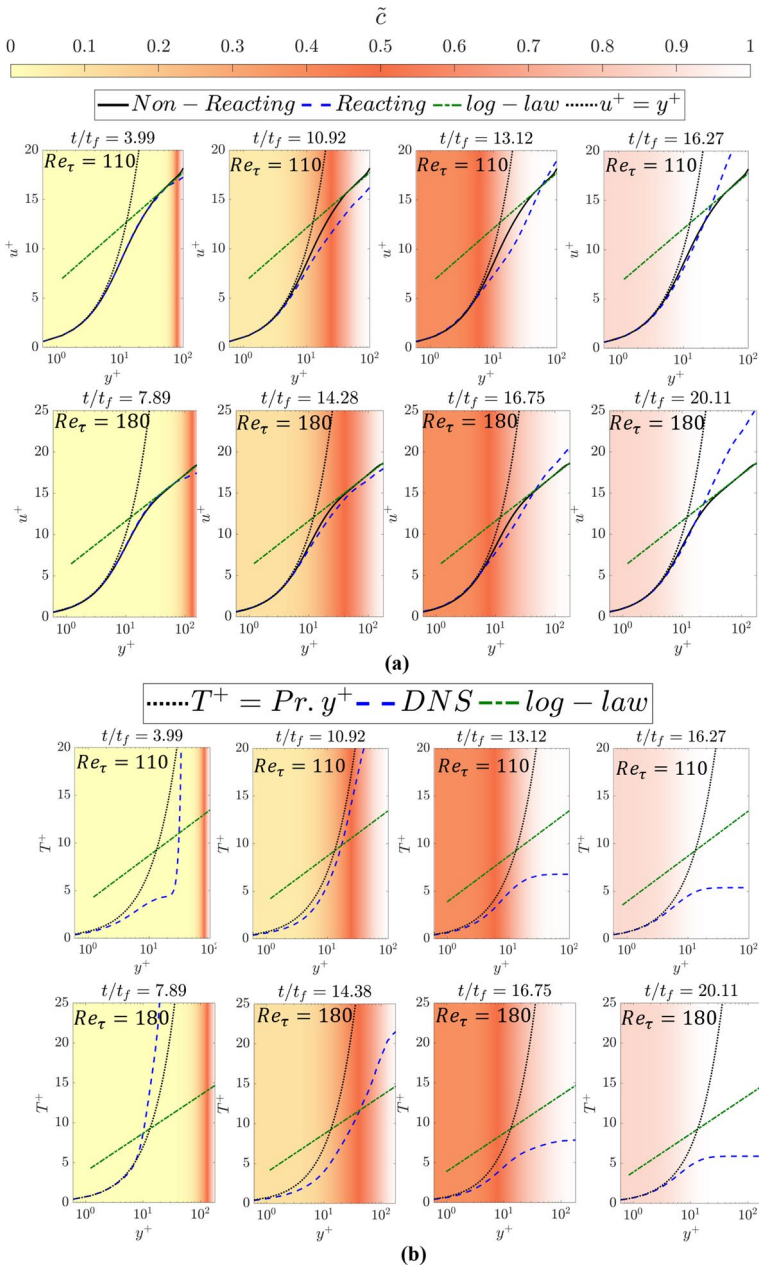
Fig. 8 Variations of (**a**) u^+ and (**b**) T^+ with y^+ at different normalised time t/t_f for the statistical planar flame HOQ case

effects are not strong, which indicates that the Boussinesq hypothesis at least predicts the correct sign of $\overline{\rho u'' v''}$ both in the fully unburned and fully burned gases. However, the value of $P_k/\overline{\rho}\tilde{\varepsilon}$ remains considerably different from unity even when the value is positive.
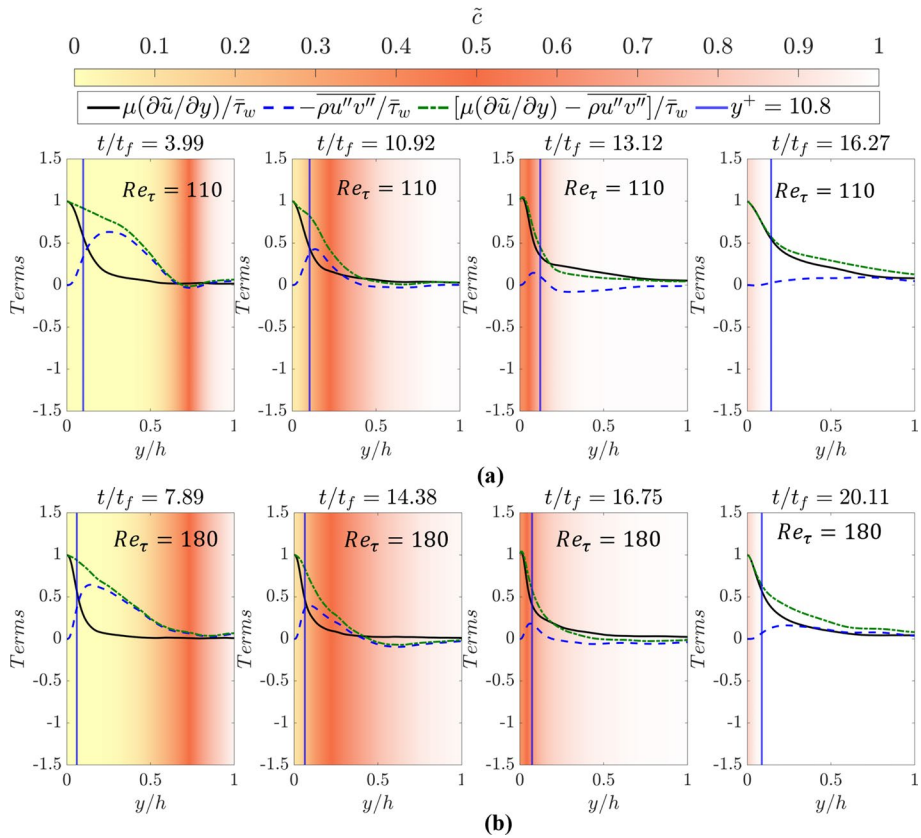
Fig. 9 Variations of $\mu(\partial\tilde{u}/\partial y)/\overline{\tau}_w$, $-\overline{\rho u''v''}/\overline{\tau}_w$ and $\left[\mu(\partial\tilde{u}/\partial y) - \overline{\rho u''v''}\right]/\overline{\tau}_w$ at different normalised time instants t/t_f for the statistical planar flame HOQ case for (**a**) $Re_\tau = 110$ and (**b**) $Re_\tau = 180$. The location corresponding to $y^+ = 10.8$ is shown by the blue vertical line

Interested readers are referred to (Ahmed et al. 2019; Ghai et al. 2023c; Lai et al. 2017a, b, c) for further discussion into the turbulent kinetic energy $\tilde{k} = 0.5\overline{\rho u_i'' u_i''}/\overline{\rho}$ transport equation during FWI in turbulent boundary layers where the physical reasons for the lack of equilibrium between P_k and $\overline{\rho}\tilde{\varepsilon}$ and the invalidity of Boussinesq's assumption in premixed turbulent FWI were discussed in detail.

The observations made from Fig. 10 suggest that Eq. 3, which was invoked during the derivation of the log-law (i.e., Eq. 5), is also rendered invalid during FWI with the reacting flow boundary layers considered here. Figures 9 and 10 show that the fundamental assumptions underpinning the derivation of the log-law (i.e., Eq. 5) are not valid during FWI within turbulent boundary layers and thus Eq. 5 is not expected to predict the variation of u^+ with y^+ accurately within the inertial layer (i.e., $y^+ > 10.8$).

The variations of $-\lambda(\partial\tilde{T}/\partial y)/\overline{q}_w$, $-\overline{\rho v''T''}/\overline{q}_w$ and $\left[-\lambda(\partial\tilde{T}/\partial y) - \overline{\rho v''T''}\right]/\overline{q}_w$ at different time instants for the HOQ of the statistically planar flame are shown in Fig. 11. The mean heat fluxes $\overline{q}_w$ are negligibly small at early times when the flame remains away from the wall (see Fig. 4) and thus the variations of $-\lambda(\partial\tilde{T}/\partial y)/\overline{q}_w$, $-\overline{\rho v''T''}/\overline{q}_w$
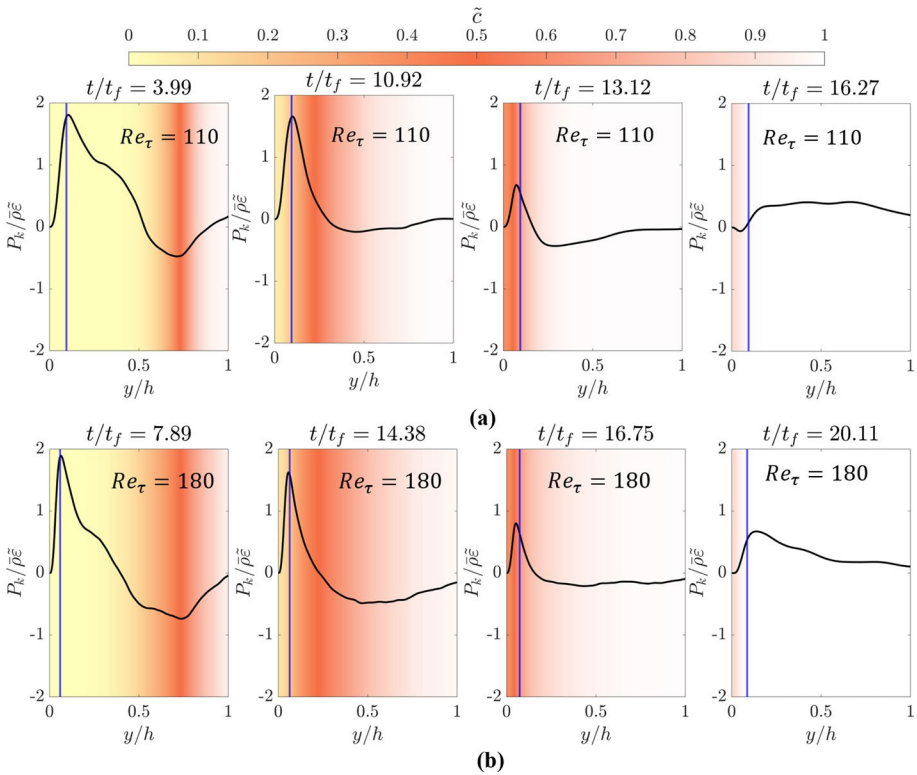
Fig. 10 Variations of $P_k/\overline{\rho}\tilde{\varepsilon}$ at different normalised time instants t/t_f for the statistical planar flame HOQ case for (**a**) $Re_\tau = 110$ and (**b**) $Re_\tau = 180$. The location corresponding to $y^+ = 10.8$ is shown by the blue vertical line

and $\left[-\lambda(\partial\tilde{T}/\partial y) - \overline{\rho v'' T''}\right]/\overline{q}_w$ at $t/t_f = 3.99$ and 7.89 for $Re_\tau = 110$ and 180, respectively are not shown in Fig. 11 to avoid any confusion. It is evident from Fig. 11 that the contribution $-\lambda(\partial\tilde{T}/\partial y)_w = \overline{q}_w$ is maintained at the wall, whereas the magnitude of $-\overline{\rho v'' T''}/\overline{q}_w$ increases in the wall normal direction. However, the magnitude of $-\overline{\rho v'' T''}/\overline{q}_w$ is significant in the intertial layer only during the initial stages of FWI, and this contribution vanishes when the flame starts to quench. Moreover, $-\lambda(\partial\tilde{T}/\partial y)$ and $-\overline{\rho v'' T''}$ exhibit same signs for a major part of the inertial layer (i.e., $y^+ > 10.8$). This suggests that the gradient hypothesis (i.e., $-\overline{\rho v'' T''} = (\overline{\rho}\nu_t/Pr_t)(\partial\tilde{T}/\partial y)$), which was assumed for the derivation of Eqs. 8 and 15 is rendered invalid for both FWI cases considered here. Furthermore, the magnitude of $\left[-\lambda(\partial\tilde{T}/\partial y) - \overline{\rho v'' T''}\right]/\overline{q}_w$ remains smaller than unity for a major part of the inertial layer (i.e., $y^+ > 10.8$) so the assumption of constant heat flux layer is rendered invalid in the case of FWI within turbulent boundary layers considered here. A comparison between Figs. 9 and 11 reveals that $\left(-\overline{\rho v'' T''}\right)$ and $-\lambda(\partial\tilde{T}/\partial y)$ exhibit the same signs (i.e. counter-gradient transport) in the regions where $\left(-\overline{\rho u'' v''}\right)$ and $\mu(\partial\tilde{u}/\partial y)$ also exhibit same signs (i.e. counter-gradient
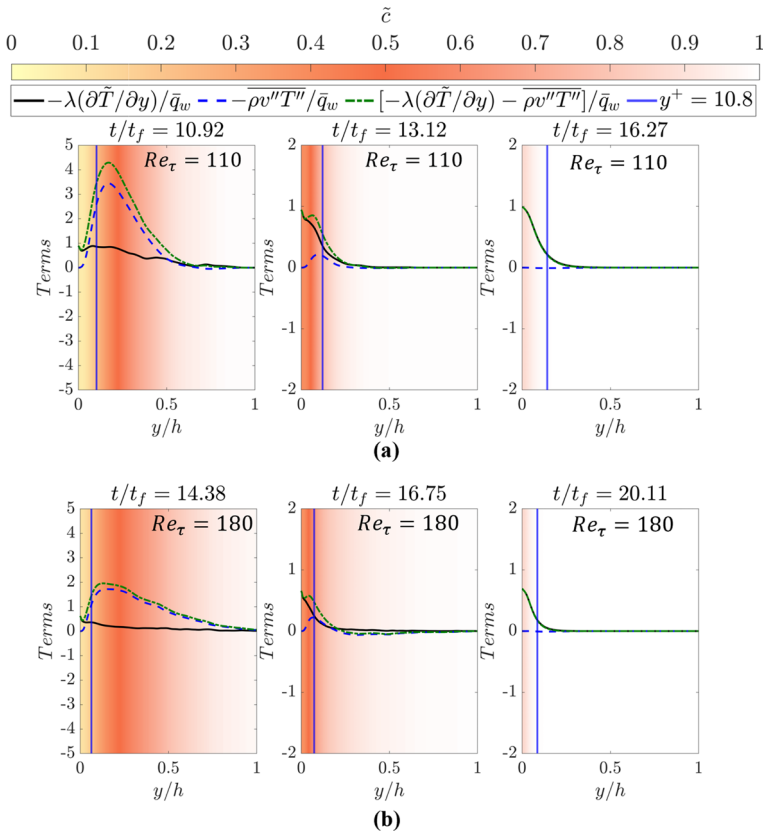
Fig. 11 Variations of $-\lambda(\partial\tilde{T}/\partial y)/\bar{q}_w$, $-\overline{\rho v''T''}/\bar{q}_w$ and $\left[-\lambda(\partial\tilde{T}/\partial y) - \overline{\rho v''T''}\right]/\bar{q}_w$ at different normalised time instants t/t_f for the statistical planar flame HOQ case for (**a**) $Re_\tau = 110$ and (**b**) $Re_\tau = 180$. The location corresponding to $y^+ = 10.8$ is shown by the blue vertical line

behaviour). Subject to the assumption of counter-gradient transport of both momentum and temperature, it is possible to obtain a log-law based relation for the mean temperature in the inertial layer if a log-law holds for the Favre-mean values of the streamwise velocity component.

4.3 Assessment of Proposed Wall Functions

Angelberger et al. (1997) and Han et al. (1996) modified the usual laws of the wall based on empirical relations given by Eqs. 21 and 22 for the purpose of FWI. The predictions of Eqs. 21 and 22 relating ψ^+ and Θ^+ in terms of η^+ are shown in Fig. 12 for the sake of completeness. The quantities η^+ and ψ^+ are approximated as $\eta^+_{Model_1} = (v_w/\tilde{v})y_1^+$ (i.e. right hand side of Eq. 17) and $\psi^+_{Model_1} = \bar{\rho}u^+/\rho_w$ (i.e. right hand side of Eq. 19) (Angelberger et al. 1997; Han et al. 1996; Poinsot and Veynante 2005) and thus the variations of $\psi^+_{Model_1}$ and Θ^+ with $\eta^+_{Model_1}$ are also shown in Fig. 12 to assess the practical implications of these approximations. Figure 12 shows that there are significant differences between the variations of ψ^+ and Θ^+ with η^+
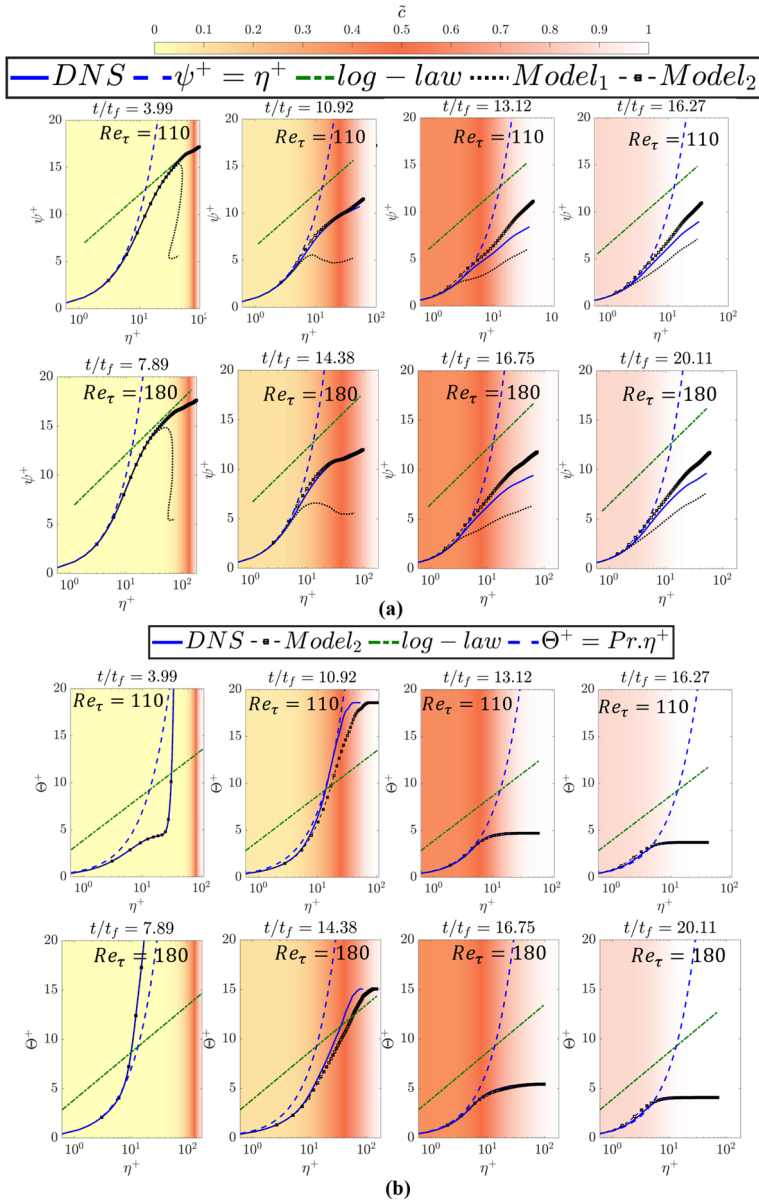
Fig. 12 Variations of (**a**) ψ^+ and (**b**) Θ^+ with η^+ at different normalised time instants t/t_f for the statistical planar flame HOQ case. The predictions of Eqs. 21 and 22 based on quantities extracted from DNS data, η^+ estimation based on Eq. 18 and η^+ estimation based on Eq. 23

with the corresponding variations of $\psi^+_{Model_1}$ and Θ^+ with $\eta^+_{Model_1}$ especially for large values of η^+. Thus, $\eta^+ \approx \eta^+_{Model_1}$ and $\psi^+ \approx \psi^+_{Model_1}$ are rendered invalid for large values of η^+. A comparison between Figs. 8 and 12 reveals that the modified wall functions given by Eqs. 20 and 21 do not offer any appreciable benefit over the standard wall functions (Eqs. 5 and 15) for the
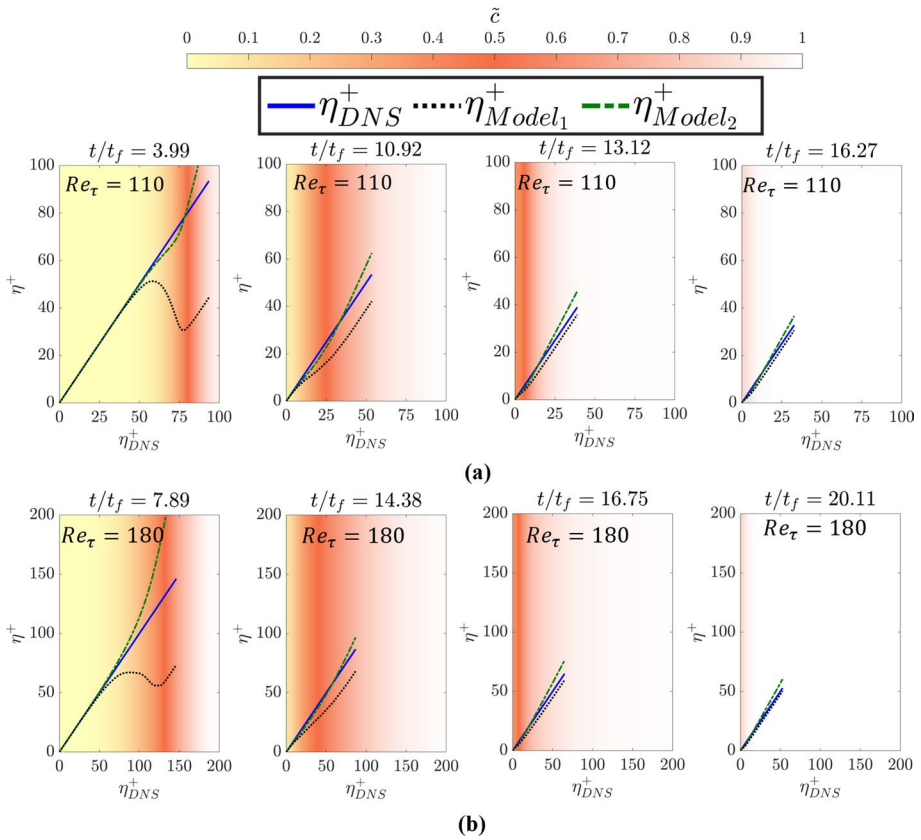
Fig. 13 Variations of η^+ obtained from Eqs. 18 and 23 (i.e. $\eta^+_{Model_1}$ and $\eta^+_{Model_2}$, respectively) with η^+ obtained from DNS data at different normalised time instants t/t_f for the statistical planar flame HOQ case for (**a**) $Re_\tau = 110$ and (**b**) $Re_\tau = 180$

inertial layer when η^+ and ψ^+ are approximated by Eqs. 18 and 19, respectively but the predictions remain in reasonable agreement with DNS data in the viscous sublayer. The variations of $\eta^+_{Model_1}$ (i.e., right hand side of Eq. 18) with η^+ obtained from DNS (i.e., left hand side of Eq. 18) for different normalised times t/t_f are shown in Fig. 13. The corresponding variations of $\psi^+_{Model_1}$ (i.e., right hand side of Eq. 19) with ψ^+ obtained from DNS (i.e., left hand side of Eq. 19) are shown in Fig. 14. It can be seen from Figs. 13 and 14 that $\eta^+_{Model_1}$ and $\psi^+_{Model_1}$ do not adequately capture the integrals $\eta^+ = \int_0^{y^+} v_w/\tilde{v}dy^+$ and $\psi^+ = \int_0^{u^+} \overline{\rho}/\rho_w du^+$. Here, $\eta^+ = \int_0^{y^+} v_w/\tilde{v}dy^+$ and $\psi^+ = \int_0^{u^+} \overline{\rho}/\rho_w du^+$ are modelled in the following manner:

$$\eta^+ = \int_0^{y^+} \frac{v_w}{\tilde{v}} dy^+ \approx (1 - \alpha_1)y^+ + \alpha_1 v_w y^+/\tilde{v} = \eta^+_{Model_2} \tag{23}$$
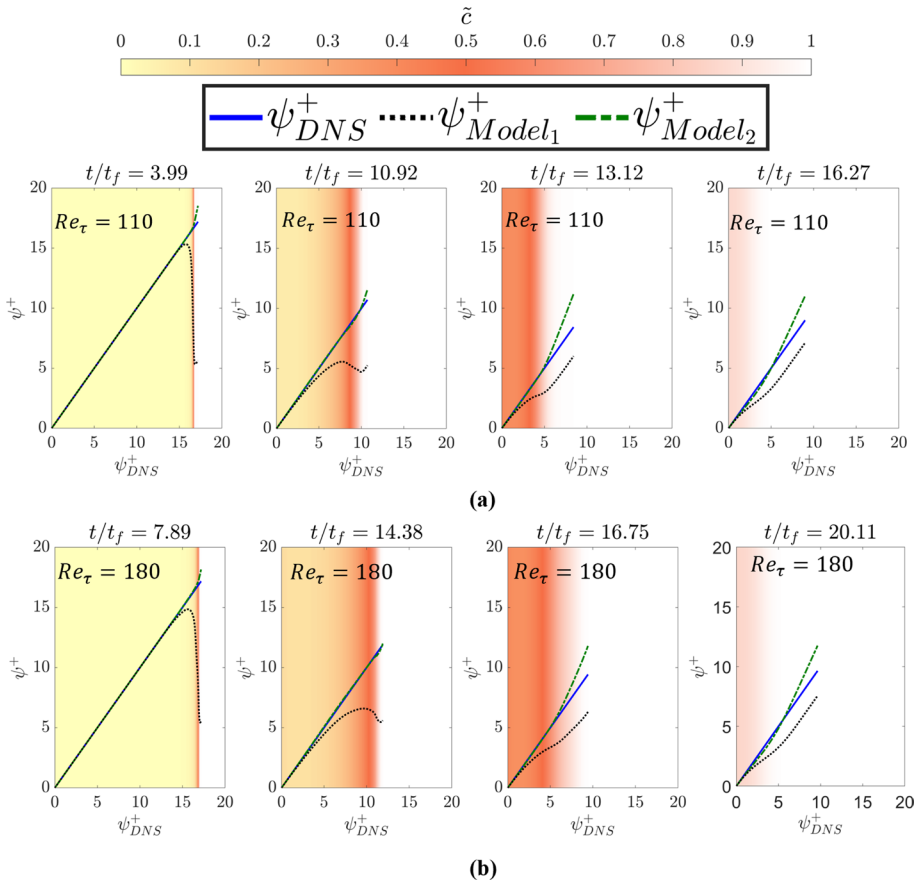
Fig. 14 Variations of ψ^+ obtained from Eqs. 19 and 24 (i.e. $\psi^+_{Model_1}$ and $\psi^+_{Model_2}$, respectively) with ψ^+ obtained from DNS data at different normalised time instants t/t_f for the statistical planar flame HOQ case for (**a**) $Re_\tau = 110$ and (**b**) $Re_\tau = 180$

$$\psi^+ = \int_0^{u^+} \frac{\overline{\rho}}{\rho_w} du^+ \approx \left(1 - \alpha_2\right) u^+ + \alpha_2 \overline{\rho} u^+ / \rho_w = \psi^+_{Model_2} \tag{24}$$

where, $\alpha_1 = \dfrac{(\tilde{c}_w - \tilde{\theta}_w)}{[(\tilde{c}_w - \tilde{\theta}_w) + \epsilon]}\left[0.5 + 0.5\text{erf}\left\{(\tilde{c}_w - \tilde{\theta}_w)^{0.2}\right\}\right]$ and

$$\alpha_2 = \frac{(\tilde{c}_w - \tilde{\theta}_w)}{[(\tilde{c}_w - \tilde{\theta}_w) + \epsilon]}\left[0.45 + 0.4\text{erf}\left\{(\tilde{c}_w - \tilde{\theta}_w)\right\}\right] \tag{25}$$

In Eq. 25, ϵ is a small number (i.e., $\epsilon < 0.0001$) to avoid division by zero. According to Eqs. 23–25, $\eta^+_{Model_2}$ and $\psi^+_{Model_2}$ approach y^+ and u^+, respectively when $(\tilde{c}_w - \tilde{\theta}_w) = 0$, which physically represents a condition when the FWI does not take place and/or when the flame remains sufficiently away from the wall to impart any influence on the near-wall dynamics.

It can be seen from Figs. 13 and 14 that $\eta^+_{Model_2}$ and $\psi^+_{Model_2}$ approximate $\eta^+ = \int_0^{y^+} \nu_w/\tilde{\nu}\,dy^+$

and $\psi^+ = \int_0^{u^+} \overline{\rho}/\rho_w du^+$ more accurately than Eqs. 18 and 19, respectively. Furthermore, the predictions of Eqs. 21 and 22, when η^+ is approximated by $\eta^+_{Model_2}$, are also shown in Fig. 13, which show that they agree with ψ^+ and Θ^+ evaluated from DNS data. This implies that Eq. 21 and 22 can be used in RANS simulations of FWI when η^+ is approximated by Eq. 23 using y^+ to obtain ψ^+ and Θ^+ and Eq. 24 can be used to obtain u^+ from ψ^+. Similarly, Eq. 20 can be used to obtain the Favre-mean temperature $\tilde{T}$ from Θ^+. It is worth noting that all the transformations for wall normal distance and mean velocity presented in Table 1 involve some degree of empiricism and the approach adopted here is no different to the earlier propositions of wall laws for the variable density flows. A degree of empiricism is not unusual in turbulence and turbulent combustion modelling and such empirical fits have a value like any new experimental or DNS result that shows an effect, which is yet to be analysed. Moreover, it has been found that Eqs. 23–25 also work well for a database of oblique wall-quenching of a V-shaped flame within a channel (Ghai et al. 2023a), which is not presented here for the sake of brevity.

5 Conclusions

The validity of the laws of the wall for Favre mean streamwise velocity component and Favre mean temperature, which are usually used for RANS simulations of non-reacting flows, has been assessed for turbulent premixed flame-wall interaction using DNS data representing unsteady head-on quenching of statistically planar flames across turbulent boundary layers. It has been found that the usual log-law based expressions for the Favre mean values of streamwise velocity and temperature for the inertial layer do not adequately capture the corresponding variations obtained from DNS data in the reacting flow turbulent boundary layers considered here. The underlying assumptions of constant shear stress and the equilibrium of production and dissipation of turbulent kinetic energy underpinning the usual log-law for the mean streamwise velocity are rendered invalid within the so-called inertial layer of the turbulent boundary layer during flame-wall interaction. Moreover, the heat flux does not remain constant within the so-called inertial layer, which along with the counter-gradient transport of temperature within the inertial layer makes the assumptions underpinning the derivation of the usual log-law for temperature to be invalid during flame-wall interaction. As several underlying assumptions are rendered invalid during FWI, a comprehensive review of various wall models is undertaken in this paper in order to assess their predictive capabilities in the presence of flame-wall interaction. It has been found that that the modified wall laws proposed by Angelberger et al. (1997) and Han et al. (1996) provided the best qualitative agreement with the variations obtained from DNS data although these expressions, which account for density and kinematic viscosity variations with temperature are empirical in nature. However, the modified wall law expressions by Angelberger et al. (1997) and Han et al. (1996) do not appreciably improve the agreement with the corresponding DNS data in the inertial layer in the reacting flow turbulent boundary layers considered here, and there is a scope for improving the way the integrations are performed while computing density-compensated velocity and kinematic viscosity compensated wall-normal coordinate in this modelling flamework. The inadequacies of the empirical modifications to the existing laws of the wall are a result of the inaccurate approximations for the kinematic viscosity compensated wall normal distance and the density compensated streamwise velocity component. The DNS data has been utilised here to

propose new expressions for the kinematic viscosity compensated wall normal distance and the density compensated streamwise velocity component, which upon using in the empirically modified law of wall expressions provide reasonable agreement with DNS data.

While the proposed modifications are incorporated in an empirical modelling framework, the modelling choices are informed by the physics extracted from the DNS data. Considering the limited information available on wall laws for flame-wall interaction, it is encouraging that the proposed modifications enhanced the predictive capabilities of wall laws for both streamwise velocity component and temperature but a theoretical framework of wall laws for flame-wall interaction based on first principles will be necessary, which will form the basis of future studies. It is also worth noting that the unity Lewis number assumption is made in this paper as a starting point because laws of the walls for FWI are rarely addressed in the existing literature. However, it has been recent demonstrated that the lack of validity of standard log-laws for streamwise velocity component and temperature for flame-wall interaction with non-unity Lewis number flames are qualitatively similar to the corresponding unity Lewis number flame (Chakraborty et al. 2023). Moreover, the modifications suggested in the current analysis in the form of Eqs. 23 and 24 do not invoke any assumptions regarding the Lewis number. Nevertheless, the predictive capabilities of the revised wall functions need to be assessed for flame-wall interaction with non-unity Lewis numbers in the future. Furthermore, the performance of newly modified wall functions needs to be assessed based on RANS simulations of premixed turbulent flame-wall interaction. Finally, the current findings need to be confirmed in the presence of detailed chemistry for the sake of completeness, although the chemical mechanism is not expected to affect turbulent flow statistics in FWI because the chemical reaction rate effects are felt through the changes in density and kinematic viscosity in turbulent flow statistics.

Appendix A

The variations of ψ^+ with η^+ at different normalised time instants t/t_f for the statistically planar flame HOQ case at $Re_\tau = 110$ and $Re_\tau = 180$ are shown in Fig. 15. The predictions from the different transformation given in Table 1 and the model approximations given by Eqs. 18, 19, 23 and 24 are also shown in Fig. 15. It can be seen from the results that within the viscous sublayer the predictions from the different transformations and the model approximations provide reasonable agreement with the standard relation i.e., given by Eq. 21. However, outside the viscous sublayer, there are significant variations in the predictions obtained from the different transformations and model approximations. The transformation proposed by Van Driest (1951) is widely used and is a classic example of density weighted velocity scaling which is based on dimensional reasoning around the mean velocity gradient in the log-layer. However, it is known to be inaccurate for non-adiabatic walls (Volpiani et al. 2020). Along with the transformation proposed by Van Driest (1951), the transformation proposed by Howarth and Taylor (1997) does not follow the inner layer similarity law given by $S_1 = S_2/(G \times H)$ (Trettel and Larsson 2016). In reacting turbulent boundary layer flows, the transformation proposed by Trettel and Larsson (2016) gives inaccurate predictions when there is a sharp change in the density ratio. The transformation given by Volpiani et al. (2020) yields satisfactorily results by collapsing mean velocity profiles with incompressible flows but their validity for the non-adiabatic turbulent boundary layer reacting flows is still questionable. However, the transformations proposed by Angelberger et al. (1997) and Han et al. (1996) provide reasonable agreement for the
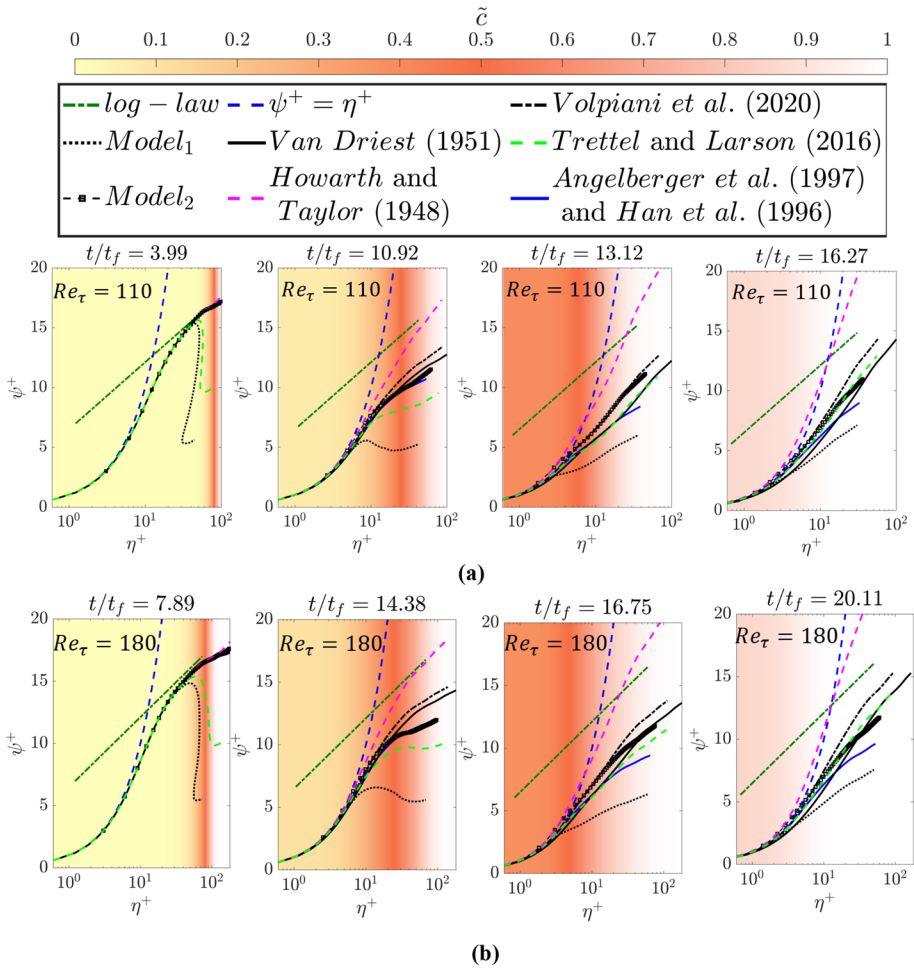
Fig. 15 Variations of ψ^+ with η^+ at different normalised time instants t/t_f for the statistical planar flame HOQ case for (**a**) $Re_\tau = 110$ and (**b**) $Re_\tau = 180$. The predictions of Eqs. 21 and 22 based on quantities extracted from DNS data, η^+ estimation based on Eq. 18 and η^+ estimation based on Eq. 23

non-adiabatic turbulent boundary layer reacting flows. Therefore, the transformations proposed by Angelberger et al. (1997) and Han et al. (1996) are used in this work as a platform to propose model modifications. The model approximations given by Eqs. 18 and 19 do not provide good collapse with the transformations proposed by Angelberger et al. (1997) and Han et al. (1996). Therefore, the new modifications given by Eqs. 23 and 24 are used which provide a reasonable collapse of mean velocity and mean temperature with the transformations proposed by Angelberger et al. (1997) and Han et al. (1996), as shown in Fig. 12.

Author Contributions NC and UA conceptualised the analysis. UA performed the simulations. NC wrote the original draft of the paper. NC and SG revised the paper. SG prepared the figures and did the analysis. NC and UA supervised SG. SG, NC, and UA reviewed the manuscript.

Declarations

Conflict of interest The authors do not have any competing interests to declare that are relevant to the content of this article.

Ethics Approval This study does not involve any research with human participants and/or animals, so no ethical approval was required.

Informed Consent This study does not involve any research with human participants animals, so no informed consent was required.

References

Ahmed, U., Doan, N.A.K., Lai, J.W., Klein, M., Chakraborty, N., Swaminathan, N.: Multiscale analysis of head-on quenching premixed turbulent flames. Phys. Fluids **30**(10), 105102 (2018)

Ahmed, U., Pillai, A.L., Chakraborty, N., Kurose, R.: Statistical behavior of turbulent kinetic energy transport in boundary layer flashback of hydrogen-rich premixed combustion. Phys. Rev. Fluids **4**(10), 103201 (2019)

Ahmed, U., Pillai, A.L., Chakraborty, N., Kurose, R.: Surface density function evolution and the influence of strain rates during turbulent boundary layer flashback of hydrogen-rich premixed combustion. Phys. Fluids **32**(5), 055112 (2020)

Ahmed, U., Chakraborty, N., Klein, M.: Assessment of bray moss Libby formulation for premixed flame-wall interaction within turbulent boundary layers: influence of flow configuration. Combust. Flame **233**, 111575 (2021a)

Ahmed, U., Apsley, D., Stallard, T., Stansby, P., Afgan, I.: Turbulent length scales and budgets of Reynolds stress-transport for open-channel flows; friction Reynolds numbers Re_τ =150, 400 and 1020. J. Hydraul. Res. **59**(1), 36–50 (2021b)

Ahmed, U., Chakraborty, N., Klein, M.: Influence of thermal wall boundary condition on scalar statistics during flame-wall interaction of premixed combustion in turbulent boundary layers. Int. J. Heat Fluid Flow **92**, 108881 (2021c)

Ahmed, U., Chakraborty, N., Klein, M.: Scalar gradient and strain rate statistics in oblique premixed flame-wall interaction within turbulent channel flows. Flow Turbul. Combust. **106**(2), 701–732 (2021d)

Ahmed, U., Chakraborty, N., Klein, M.: Influence of flow configuration and thermal wall boundary conditions on turbulence during premixed flame-wall interaction within low reynolds number boundary layers. Flow Turbul. Combust. **111**, 825 (2023a)

Ahmed, U., Malkeson, S.P., Pillai, A.L., Chakraborty, N., Kurose, R.: Flame self-interaction during turbulent boundary layer flashback of hydrogen-rich premixed combustion. Phys. Rev. Fluids **8**(2), 023202 (2023b)

Alshaalan, T. M., and Rutland, C. J.: Turbulence, scalar transport, and reaction rates in flame-wall interaction. *Twenty-Seventh Symposium (International) on Combustion, 27*(1), 793–799 (1998)

Alshaalan, T., Rutland, C.J.: Wall heat flux in turbulent premixed reacting flow. Combust. Sci. Technol. **174**(1), 135–165 (2002)

Angelberger, C., Poinsot, T., and Delhay, B.: Improving Near-Wall Combustion and Wall Heat Transfer Modeling in SI Engine Computations. Int. Fall Fuels and Lub. Meet. and Expo., SAE paper, 972881 (1997)

Bruneaux, G., Akselvoll, K., Poinsot, T., Ferziger, J.H.: Flame-wall interaction simulation in a turbulent channel flow. Combust. Flame **107**(1–2), 27–36 (1996)

Bruneaux, G., Poinsot, T., Ferziger, J.H.: Premixed flame-wall interaction in a turbulent channel flow: budget for the flame surface density evolution equation and modelling. J. Fluid Mech. **349**, 191–219 (1997)

Chakraborty, N., Katragadda, M., Cant, R.S.: Effects of Lewis number on turbulent kinetic energy transport in premixed flames. Phys. Fluids **23**(7), 075109 (2011a)

Chakraborty, N., Katragadda, M., Cant, R.S.: Statistics and modelling of turbulent kinetic energy transport in different regimes of premixed combustion. Flow Turbul. Combust. **87**(2), 205–235 (2011b)

Chakraborty, N., Ghai, S. K., and Ahmed, U.: Effects of fuel lewis number on turbulent flow statistics in oblique-wall quenching of premixed v-shaped flames within turbulent channel flows. In: 14th International ERCOFTAC symposium on engineering turbulence modelling and measurements, Barcelona, Spain (2023)

Durbin, P.A., Pettersson Reif, B.A.: Statistical Theory and Modeling for Turbulent Flows. Wiley (2010)

Ghai, S.K., Ahmed, U., Chakraborty, N., Klein, M.: Entropy generation during head-on interaction of premixed flames with inert walls within turbulent boundary layers. Entropy **24**(4), 463 (2022a)

Ghai, S.K., Ahmed, U., Klein, M., Chakraborty, N.: Energy integral equation for premixed flame-wall interaction in turbulent boundary layers and its application to turbulent burning velocity and wall flux evaluations. Int. J. Heat Mass Transf. **196**, 123230 (2022b)

Ghai, S.K., Chakraborty, N., Ahmed, U., Klein, M.: Enstrophy evolution during head-on wall interaction of premixed flames within turbulent boundary layers. Phys. Fluids **34**(7), 075124 (2022c)

Ghai, S.K., Ahmed, U., Chakraborty, N.: Effects of fuel lewis number on wall heat transfer during oblique flame-wall interaction of premixed flames within turbulent boundary layers. Flow Turbul. Combust. **111**(3), 867–895 (2023a)

Ghai, S.K., Ahmed, U., Chakraborty, N.: Statistical behaviour and modelling of variances of reaction progress variable and temperature during flame-wall interaction of premixed flames within turbulent boundary layers. Flow Turbul. Combust. (2023b). https://doi.org/10.1007/s10494-023-00439-w

Ghai, S.K., Ahmed, U., Klein, M., Chakraborty, N.: Turbulent kinetic energy evolution in turbulent boundary layers during head-on interaction of premixed flames with inert walls for different thermal boundary conditions. Proc. Combust. Inst. **39**(2), 2169–2178 (2023c)

Gruber, A., Sankaran, R., Hawkes, E.R., Chen, J.H.: Turbulent flame-wall interaction: a direct numerical simulation study. J. Fluid Mech. **658**, 5–32 (2010)

Gruber, A., Chen, J.H., Valiev, D., Law, C.K.: Direct numerical simulation of premixed flame boundary layer flashback in turbulent channel flow. J. Fluid Mech. **709**, 516–542 (2012)

Han, Z., Reitz, R.D., Corcione, F.E., Valentino, G.: Interpretation of k-ε computed turbulence length-scale predictions for engine flows. Symp. Combust. **26**(2), 2717–2723 (1996)

Hanjalić, K., Launder, B.: Modelling Turbulence in Engineering and the Environment: Second-Moment Routes to Closure. Cambridge University Press (2011)

Howarth, L., Taylor, G.I.: Concerning the effect of compressibility on lam inar boundary layers and their separation. Proc. r. Soc. London Ser. A Math. Phys. Sci. **194**(1036), 16–42 (1997)

Jainski, C., Rissmann, M., Bohm, B., Dreizler, A.: Experimental investigation of flame surface density and mean reaction rate during flame-wall interaction. Proc. Combust. Inst. **36**(2), 1827–1834 (2017a)

Jainski, C., Rissmann, M., Bohm, B., Janicka, J., Dreizler, A.: Sidewall quenching of atmospheric laminar premixed flames studied by laser-based diagnostics. Combust. Flame **183**, 271–282 (2017b)

Jainski, C., Rissmann, M., Jakirlic, S., Bohm, B., Dreizler, A.: Quenching of premixed flames at cold walls: effects on the local flow field. Flow Turbul. Combust. **100**(1), 177–196 (2018)

Jenkins, K. W., and Cant, R. S.:. Direct numerical simulation of turbulent flame kernels. In D. Knight and L. Sakell, Recent Advances in DNS and LES, Dordrecht (1999)

Jiang, B., Gordon, R.L., Talei, M.: Head-on quenching of laminar premixed methane flames diluted with hot combustion products. Proc. Combust. Inst. **37**(4), 5095–5103 (2019)

Jiang, B., Brouzet, D., Talei, M., Gordon, R.L., Cazeres, Q., Cuenot, B.: Turbulent flame-wall interactions for flames diluted by hot combustion products. Combust. Flame **230**, 111432 (2021)

Kawamura, H., Ohsaka, K., Abe, H., Yamamoto, K.: DNS of turbulent heat transfer in channel flow with low to medium-high Prandtl number fluid. Int. J. Heat Fluid Flow **19**(5), 482–491 (1998)

Kays, W.M., Crawford, M.E.: Convective Heat and Mass Transfer, 3rd edn. New York, McGraw-Hill (1993)

Kim, J., Moin, P., Moser, R.: Turbulence statistics in fully developed channel flow at low Reynolds number. J. Fluid Mech. **177**, 133–166 (1987)

Kitano, T., Tsuji, T., Kurose, R., Komori, S.: Effect of pressure oscillations on flashback characteristics in a turbulent channel flow. Energy Fuels **29**(10), 6815–6822 (2015)

Konstantinou, I., Ahmed, U., Chakraborty, N.: Effects of fuel lewis number on the near-wall dynamics for statistically planar turbulent premixed flames impinging on inert cold walls. Combust. Sci. Technol. **193**(2), 235–265 (2020)

Lai, J., Chakraborty, N.: Effects of lewis number on head on quenching of turbulent premixed flames: a direct numerical simulation analysis. Flow Turbul. Combust. **96**(2), 279–308 (2016a)

Lai, J., Chakraborty, N.: A priori direct numerical simulation modeling of scalar dissipation rate transport in head-on quenching of turbulent premixed flames. Combust. Sci. Technol. **188**(9), 1440–1471 (2016b)

Lai, J., Moody, A., Chakraborty, N.: Turbulent kinetic energy transport in head-on quenching of turbulent premixed flames in the context of Reynolds Averaged Navier Stokes simulations. Fuel **199**, 456–477 (2017a)

Lai, J., Alwazzan, D., Chakraborty, N.: Turbulent scalar flux transport in head-on quenching of turbulent premixed flames: a direct numerical simulations approach to assess models for Reynolds averaged Navier Stokes simulations. J. Turbul. **18**(11), 1033–1066 (2017b)

Lai, J., Chakraborty, N., Lipatnikov, A.: Statistical behaviour of vorticity and enstrophy transport in head-on quenching of turbulent premixed flames. Eur. J.mech. B-Fluids **65**, 384–397 (2017c)

Lai, J., Klein, M., Chakraborty, N.: Direct numerical simulation of head-on quenching of statistically planar turbulent premixed methane-air flames using a detailed chemical mechanism. Flow Turbul. Combust. **101**(4), 1073–1091 (2018)

Lai, J., Ahmed, U., Klein, M., Chakraborty, N.: A comparison between head-on quenching of stoichiometric methane-air and hydrogen-air premixed flames using Direct Numerical Simulations. Int. J. Heat Fluid Flow **93**, 108896 (2022)

Mann, M., Jainski, C., Euler, M., Bohm, B., Dreizler, A.: Transient flame-wall interactions: experimental analysis using spectroscopic temperature and CO concentration measurements. Combust. Flame **161**(9), 2371–2386 (2014)

Nishiki, S., Hasegawa, T., Borghi, R., Himeno, R.: Modeling of flame-generated turbulence based on direct numerical simulation databases. Proc. Combust. Inst. **29**, 2017–2022 (2002)

Peters, N.: Turbulent Combustion, Ist Cambridge University Press (2000)

Poinsot, T., Veynante, D.: Theoretical and numerical combustion, 2nd edn. Edwards Inc (2005)

Poinsot, T.J., Haworth, D.C., Bruneaux, G.: Direct simulation and modeling of flame-wall interaction for premixed turbulent combustion. Combust. Flame **95**(1–2), 118–132 (1993)

Pope, S.B.: Turbulent Flows. Cambridge University Press (2000)

Rißmann, M., Jainski, C., Mann, M., Dreizler, A.: Flame-flow interaction in premixed turbulent flames during transient head-on quenching. Flow Turbul. Combust. **98**(4), 1025–1038 (2016)

Sellmann, J., Lai, J.W., Kempf, A.M., Chakraborty, N.: Flame surface density based modelling of head-on quenching of turbulent premixed flames. Proc. Combust. Inst. **36**(2), 1817–1825 (2017)

Smooke, M.D., Giovangigli, V.: Extinction of tubular premixed laminar flames with complex chemistry (1991).

Trettel, A., Larsson, J.: Mean velocity scaling for compressible wall turbulence with heat transfer. Phys. Fluids **28**(2), 026102 (2016)

Tsukahara, T., Seki, Y., Kawamura, H., and Tochio, D.: DNS of turbulent channel flow at very low Reynolds numbers. In Proc. of the Forth Int. Symp. on Turbulence and Shear Flow Phenomena, pp. 935–940 (2005)

Van Driest, E.R.: Turbulent boundary layer in compressible fluids. J. Aeronautical Sci. **18**(3), 145–160 (1951)

Volpiani, P.S., Iyer, P.S., Pirozzoli, S., Larsson, J.: Data-driven compressibility transformation for turbulent wall layers. Phys. Rev. Fluids **5**(5), 052602 (2020)

Wilcox, D.C.: Turbulence Modeling for CFD. DCW Industries (1998)

Yoo, C.S., Im, H.G.: Characteristic boundary conditions for simulations of compressible reacting flows with multi-dimensional, viscous and reaction effects. Combust. Theor. Model. **11**(2), 259–286 (2007)

Zhao, P.P., Wang, L.P., Chakraborty, N.: Analysis of the flame-wall interaction in premixed turbulent combustion. J. Fluid Mech. **848**, 193–218 (2018a)

Zhao, P.P., Wang, L.P., Chakraborty, N.: Strain rate and flame orientation statistics in the near-wall region for turbulent flame-wall interaction. Combust. Theor. Model. **22**(5), 921–938 (2018b)

Zhao, P.P., Wang, L.P., Chakraborty, N.: Vectorial structure of the near-wall premixed flame. Phys. Rev. Fluids **4**(6), 063203 (2019)

Zhao, P.P., Wang, L.P., Chakraborty, N.: Effects of the cold wall boundary on the flame structure and flame speed in premixed turbulent combustion. Proc. Combust. Inst. **38**(2), 2967–2976 (2021)